Prediction of Meat Quality: application of hyperspectral imaging and Raman spectroscopy

Bruce W. Moss[a], Astor Chau[b], Martin B. Whitworth[b], J. Rene Beattie[c], Ann Fearon[a] and Alan Gordon[a]

[a]Agri-Food & Biosciences Institute, Newforge Lane, Belfast BT9 5PX
[b]Campden BRI, Station Road, Chipping Campden, Gloucestershire, GL55 6LD.
[c]Department of Vision Science, Queens University of Belfast,

Summary

This project investigated the potential application of two spectral approaches - hyperspectral imaging in the near infrared (NIR) region and Raman spectroscopy - to predict meat quality. Predictions of meat quality included Warner-Bratzler shear force (WBSF), consumer assessed eating quality and fatty acid profiles. In addition, the relationship between WBSF values and sensory acceptability was evaluated using logistic regression.

NIR hyperspectral imaging showed that, by using an absorbance band at a specific range of wavelengths, the areas corresponding to lean and fat (marbling fat, intermuscular fat and subcutaneous fat) could be clearly identified. The distribution of fat and lean in an image of the forerib produced using spectral characteristics was almost identical to that seen in a colour image taken with a digital camera (Nikon D70). Prediction models for meat quality were developed based on the spectral characteristics of the total *longissimus dorsi* (LD) muscle surface, including areas of marbling fat, and also on the spectral characteristics of the LD lean regions alone, excluding spectral characteristics of the marbling fat. The spectral characteristics of the marbling fat were used to predict fatty acid profiles in the muscle. Prediction models were developed by using spectral data sets of both unbloomed and bloomed samples independently, and combined spectra of both bloomed and unbloomed samples.

Prediction of Warner-Bratzler Shear Force (WBSF) using the total LD area (including marbling) was marginally better when the bloomed spectra were used ($R^2 = 0.61$ WBSF at 14 day aging: $R^2 = 0.49$ WBSF at 21 day aging) than when the unbloomed or combined spectra were used. Using the total LD spectra, prediction of eating quality attributes at 14 days aging ranged from $R^2 = 0.44$ for overall liking (bloomed spectra) to $R^2 = 0.53$ for juiciness (bloomed spectra). The coefficients of determination (R^2) for prediction models developed using the spectra of the LD lean (excluding marbling fat) were generally of a similar order to the models developed using the spectra of the total LD.

The spectra of the total LD (including marbling) resulted in good prediction of intramuscular fat (IMF), with the best prediction model obtained using the unbloomed samples ($R^2 = 0.74$). Using the total LD spectra the best prediction model for total saturated fatty acids (SFA) ($R^2 = 0.68$) was obtained from the combined (unbloomed and bloomed) spectra model, whilst the best prediction of total monounsaturated fatty acids (MUFA) ($R^2 = 0.80$) was obtained from unbloomed samples. Prediction of total polyunsaturated fatty acids (PUFA) and

conjugated linoleic acid (CLA) using the total LD spectra was generally poorer than for SFA and MUFA.

The prediction models for most fatty acid groups such as SFA, MUFA and CLA obtained from the spectra of the marbling fat were improved by using the spectra with identified marbling fat with an area more than 50 pixels ($R^2 = 0.66$ SFA, $R^2 = 0.58$ MUFA and $R^2 = 0.65$ CLA). However, this did not improve the R^2 value in the prediction model for PUFA ($R^2 = 0.48$) for which the best result was obtained from the unbloomed spectra ($R^2 = 0.53$). The use of identified marbling fat with an area more than 50 pixels generally eliminated the factors such as noise, misclassified pixels and also the fat adhering to the meat surface.

Using Raman spectroscopy, prediction of WBSF values and consumer assessed eating quality was poor. The only statistically significant model was the prediction of juiciness, which only explained 9% of the variation in the data ($R^2 = 0.09$). Raman spectroscopy showed greater potential for the prediction of intramuscular fat content ($R^2 = 0.23$), marbling score ($R^2 = 0.41$), MUFA ($R^2 = 0.26$), SFA ($R^2 = 0.25$) and CLA ($R^2 = 0.19$). The low prediction ability of the Raman spectra to predict quality aspects may be due to the spectrometer not operating optimally. The reasons for this are discussed in the report.

A statistically significant logistic regression model was developed which showed that consumers in the trial rated LD muscle with a WBSF value of 5.4 kg force or less as 70% acceptable. Possible reasons for the difference between the current study and a US study where consumers found meat with 5.4 kg force to be only 30% acceptable are discussed.

1 Introduction

Several workers have studied the application of near infrared spectroscopy (NIRS) to the prediction of meat quality (for recent review see Prieto *et al.* 2009). Prieto *et al.* (2009) concluded that NIR was much better at predicting meat composition (fat, protein and water) than meat quality (WBSF and tenderness etc.). Evaluation of equipment designed for on-line application in the US (Shackelford *et al.* 2004 and 2005) did not yield reliable prediction models when tested in the UK (Moss *et al.* 2009). One major difference between carcasses in the US and the UK is the greater degree of marbling fat in the ribeye in the US compared to the UK. The equipment designed in the US (ASD Boulder, Colorado) measures a relatively large area (30 mm diameter) of meat compared to previous reflectance probes; however, the average spectrum obtained from this measurement will be influenced by the amount of marbling fat in the area measured. Hyperspectral imaging provides a potential technique to differentiate the marbling fat from the lean tissue. In hyperspectral imaging, the individual spectra may cover an area as small as 1 mm^2, depending on the resolution of the imaging camera. Naganathan *et al.* (2008) used hyperspectral imaging in the visible / NIR region (400 – 1000 nm) to classify beef ribeye successfully into tenderness classes based on slice shear force values. Naganathan *et al.* (2008) did not, however, attempt to use the imaging process to separate lean tissue from marbling fat and thus the amount of marbling fat is a component of their prediction model.

Raman spectroscopy measures similar molecular vibrations to NIR. However, unlike NIR, it does not have strong absorption spectra for water and, in general, produces more spectral information than NIR, particularly in relation to protein structure. There are relatively few studies on the application of Raman spectroscopy to meat. This has been partly due to the high cost of Raman spectrometers and the sensitivity of detectors required. Raman spectroscopy involves shining a laser on the sample and measuring the scattered light. A small number of molecules become excited and it is this energy change in the scattered light (Stoke's scattering) that is measured in Raman spectroscopy. The wavelength change in the scattered light due to excitation of the molecules is dependent on the molecules present. The Stoke's scattering is several orders of magnitude less than light scattered without any wavelength change, so that extremely sensitive detectors are required, and this has added to the cost of Raman equipment.

Raman spectroscopy has shown the potential to predict fatty acid profiles in adipose tissue from a range of species (Beattie *et al.* 2006a and 2007). Beattie *et al.* (2004b) showed that Raman spectroscopy could be used to predict eating quality of beef silverside. In this case, however, the Raman spectra were acquired at the same time as the measurements of eating quality. A relationship between Raman spectra and WSBF values for pork was based on samples where the Raman spectra and WBSF values were measured at different times of aging post mortem (Beattie *et al.* 2008). The potential of Raman spectra measured at 2 or 3 days post slaughter to predict meat quality at later times post slaughter (e.g. 14 or 21 day aging) has not been evaluated.

A number of studies have shown the ability of NIR measurements of meat to predict fatty acid profiles (Realini *et al.* 2004, González-Martín *et al.*, 2005). It is difficult to identify specific features in the NIR spectra that might relate to molecular characteristics of fatty acids (e.g. unsaturated bonds, chain length), whereas these molecular features are clearly evident in Raman Spectra (Beattie *et al.* 2004a).

Since NIR is very good at predicting compositional aspects, it is possible that the ability to predict individual fatty acids may be due to the fact that these individual fatty acids are highly correlated with intramuscular fat content. The ability of NIR to predict fatty acid profiles over a wide range of diets which may change fatty acid profiles has not been demonstrated. With hyperspectral imaging it is possible to identify those parts of the image that are fat - either intermuscular or intramuscular (marbling) fat. Hyperspectral imaging thus has the potential to predict fatty acid profiles from the spectra of fat rather than lean with only a small percentage of fat.

2 Objectives

The following are the main objectives of the project:

1. To determine the potential of NIR hyperspectral imaging measured at 2 days post slaughter to:
   i. differentiate spectra of fat and lean in meat joints
   ii. predict WBSF at 14 days post mortem
   iii. predict fatty acid profiles
   iv. predict eating quality evaluated by consumers at 14 days post mortem
2. To determine the potential of Raman spectra measured at 2 days post mortem to:
   i. predict WSBF at 14 and 21 days post slaughter
   ii. predict eating quality evaluated by consumers at 14 days post slaughter
3. To determine the relationship between WBSF values and consumer acceptability at 14 days post slaughter.

The standard instrumental method for measurement of meat tenderness is WBSF. Several papers have shown that WBSF is a good predictor of tenderness as measured by sensory assessment. Platter *et al.* (2003) derived a relationship between WBSF and the probability of the acceptability of tenderness. There are no studies in the UK comparable to those of Platter *et al.* (2003).

3 Experimental

3.1 Sample preparation

A total of 164 animals (59 bulls, 54 heifers and 51 steers) were selected at random from a commercial abattoir. The carcasses were selected over a period of 2 days (Tuesday and Wednesday) in the first week in September, and from 3 days (Monday, Tuesday and Wednesday) 3 weeks later. All carcasses selected were hung by the Achilles tendon. Two days post slaughter a forerib joint from the left side of each animal was removed and taken to the laboratory for hyperspectral NIR imaging, Raman spectroscopy and instrumental analysis of meat quality. The forerib was stored in the chiller at 2^{o}C until required for hyperspectral imaging (section 3.2) and sampling for Raman analysis (section 3.3) and fatty acid analysis (section 3.5).

In order to obtain standard sample height for focussing of the hyperspectral image, a slice was removed from the anterior end of all foreribs to give a total length of 230 ± 10 mm. To prepare the samples for hyperspectral imaging a saw cut was made through the ribs at about 25 mm from the exposed caudal surface (surface exposed at quartering point). Care was taken with this saw cut not to cut into the lean meat muscle within the forerib. Immediately prior to hyperspectral imaging, the initial saw cut was completed using a steak knife to remove a slice of approximately 25 mm from the caudal end of the forerib. This resulted in a freshly cut surface and a trimmed forerib length of 230 ± 10 mm to enable the cut surface to be presented at a consistent position in the imaging system, providing consistent magnification and focus. Hyperspectral images were collected on the freshly cut surface within 2 minutes of exposing the freshly cut surface.

After scanning with the hyperspectral imaging system the samples were then removed from the apparatus, placed in a loose fitting polythene bag to allow the surface to bloom but not dry out, and returned to the chill room for at least one hour. After 1 hour, the forerib was removed from chill room and a further hyperspectral image of the bloomed surface obtained.

After the hyperspectral imaging measurements were complete the marbling of the bloomed surface, nearest to the quartering point (i.e. same surface as used for hyperspectral imaging), was assessed visually using photographic standards from Meat Standards Australia. These standards range from 200 (low marbling) to 1100 (high marbling) in steps of 100. Intermediate values are assessed subjectively depending on both the amount and distribution of marbling within the LD. Following assessment of marbling the LD muscle was removed from the forerib, cut into 25 mm slices and vacuum packed. These slices were stored and chilled until measurement of WBSF at 14 and 21 days post slaughter.

The initial 25 mm slice removed from the forerib was dissected into the fat and LD muscle. The Raman spectra were measured on the LD portion of the slice, which was then vacuum packed and blast frozen for fatty acid analysis. A sample of fat was also frozen for fatty acid analysis.

The sirloin from each carcass was removed at 2 days post slaughter for consumer evaluation of eating quality, vacuum packed at the factory and taken to the laboratory where it was

stored in a chiller at 2°C until 14 days post slaughter. At this time the sirloin was prepared for consumer assessment (section 3.4).

Figure 1 – Hyperspectral NIR imaging system

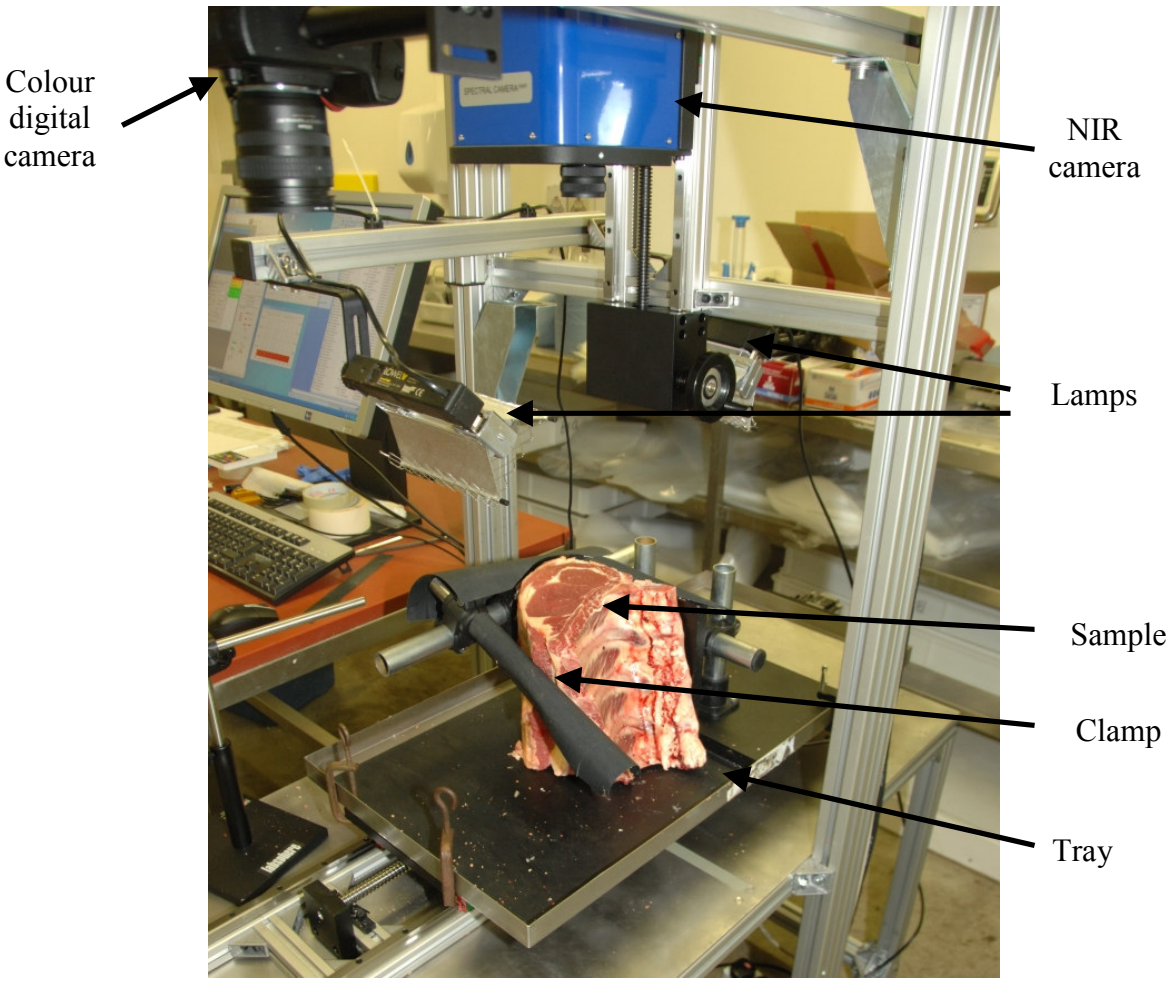

3.2 Hyperspectral NIR imaging

Hyperspectral NIR imaging was used to take images of cut surfaces of foreribs, with an NIR spectrum at each point in the sample. The data were analysed to identify lean and fat regions and to calculate mean spectra for each. The spectral data for all the samples were compared with reference measurements of texture and fat composition to develop predictions for these attributes.

NIR hyperspectral images were taken using a system described by Millar *et al.* (2008), illustrated in Figure 1. The system was supplied by Gilden Photonics Ltd. (Glasgow, U.K.) and includes a SWIR spectral camera (Specim Ltd., Oulu, Finland) containing a cooled 14 bit 320×256 pixel HgCdTe detector and N25E spectrograph. This is mounted above a motorised translation stage, operating in a 'pushbroom' configuration. The system takes an image of a line across the sample, spanning the 320 pixel width of the sensor, and the spectrograph spreads the spectra for each of these pixels across the other dimension of the sensor, spanning 240 of the available 256 pixels in this direction. Samples are then translated to collect data for further lines, resulting in a data cube consisting of two spatial dimensions and one

wavelength dimension, containing spectra for each point on the exposed sample surface. The camera and translation stage were controlled and data captured using SpectralCube 3.0041 software (Specim).

Beef samples were placed on a tray attached to the translation stage of the hyperspectral imaging equipment (Figure 1), clamped in position with the freshly cut surface uppermost and scanned with the imaging system. Samples were then removed from the apparatus, placed in a loose fitting polythene bag to allow the surface to bloom but not dry out, and returned to the chill room for at least one hour. After 1 hour, the forerib was removed from chill room and a further hyperspectral image of the bloomed surface obtained.

The base of the tray was lined with a black painted board, and the clamps were covered with black material to provide good contrast with the sample. The sample was illuminated with two 500 W incandescent lamps and imaged with a 22.5 mm lens to give a field of view with a measured width ('swathe') of 200 mm in the plane of the sample surface and a resolution of 0.625 mm pixel^{-1}. To minimise heating of the sample by the lamps, these were only turned on for the duration of the scan.

Scans were taken at a camera frequency of 50 frames s^{-1} and the translation stage was driven at a speed of 31.25 mm s^{-1} to provide the same vertical and horizontal resolution. The stage was moved through a distance of typically 250 to 290 mm, sufficient to scan the whole sample, requiring a scan time of 8 to 9 s. The camera shutter was automatically closed at the end of each scan and several frames were recorded to establish the baseline signal of the detector. For each batch of samples, a scan was also taken of a white PTFE reference material with approximately 100% reflectance across the entire measured spectral range.

The signal strength can be controlled by specifying the integration time used to capture each frame. For beef samples, the reflectance of intermuscular fat was much greater than that of lean muscle and marbling fat. Higher integration times result in a stronger signal for muscle, but saturation of some spectral bands for intermuscular fat. An integration time of 5 ms was initially selected, based on preliminary tests of additional beef samples, to provide a suitable compromise between maximising the signal strength for measurement of lean spectra and minimising the number of saturated intermuscular fat pixels. During analysis of the actual samples, this was found to result in greater saturation of intermuscular fat than intended. For most of the samples, two scans were therefore made, using exposure times of 4 ms and 5 ms, the latter for consistency with the scans already made and the former to reduce the saturation. In practice, the data for intermuscular fat were not used for generation of predictions and both sets of scans were used. The order in which the 4 ms and 5 ms scans were made was alternated throughout the experiments. For future work, if it were known that data were not required for intermuscular fat, longer integration times could be used to increase the signal strength further.

For reference purposes, a colour image of each sample was taken after each NIR scan. A digital camera was mounted alongside the NIR camera as shown in Figure 1. After NIR scanning, the sample was moved to a position directly underneath the digital camera, using the translation stage, and an image was taken. A Munsell Mini ColorChecker® chart (X-

Rite) with 24 colour patches was placed alongside the sample to aid comparison of colour between samples.

3.3 Raman spectroscopy

Raman spectra were measured using a Perkin Elmer RamanStation 400 with an excitation laser wavelength of 785 nm. For each sample an overall spectrum was obtained by co-adding spectra from a matrix of 5 x 5 sample points, separated by 5 mm between points. Each point within the matrix was the sum of 2 exposures of 30s acquisition. The signal arising from the instrument optics was obtained prior to each sample and the sample was focussed at the first sampling point. All spectra were examined for presence of cosmic spikes and any spikes were removed used a routine developed by J.R. Beattie for use in Matlab (The Mathworks). Correction for background fluorescence was undertaken using an algorithm developed by Beattie using Matlab software.

3.4 Consumer assessment

At 14 days post slaughter the LD muscle was removed from the sirloins and trimmed of external fat and connective tissues. Slices 25 mm thick were removed from the anterior end of the LD and each slice was cut into pieces of approximately 50 mm square. Each piece was wrapped in food grade film and the wrapped pieces were vacuum packed in five pieces to a pack. One pack of five was blast frozen at 14 days post slaughter; the other pack was held in a chiller until 21 days post slaughter when it was also blast frozen for consumer analysis. Sensory assessment involved a total of 240 consumers obtained through charities and social clubs. The samples required for assessment were allowed to thaw for 24 hours at 4 ^{o}C. Samples were then cooked for 6.5 minutes on a clam type grill (Silesia). This cooking procedure resulted in a well done steak (Farmer *et al.* 2009a).

Each consumer was presented with 7 samples, the first of which was not included in the experiment. The 6 experimental samples presented were balanced for sex type and aging period. The consumers assessed the samples for tenderness, juiciness, flavour and overall liking using a line scale. The consumers also assessed acceptability as a yes/no decision and quality score as unacceptable, everyday quality, better than everyday quality and premium quality.

3.5 Fatty Acid Analysis

Lipid was extracted from minced meat using a standard chloroform/methanol extraction method (Bligh and Dyer, 1959) and was dissolved in hexane. The fatty acid composition was determined using capillary column gas-liquid chromatography (GC) following preparation of the fatty acids as methyl esters (FAME) using methanolic KOH as described in BS 684-2.34 (2001). An aliquot (1.0 μl) of the FAME was injected onto a capillary column (0.25 mm id, 120 m length), WCOT fused silica-coated BPX70 (Phenomenex Cheshire, UK), in a Varian Star 3800 gas chromatograph (Varian Associates Ltd., Walton-on-Thames, UK) equipped with a temperature programmable injector operated in the split mode and a flame ionisation detector (FID). The column temperature was programmed from 50^{o}C to 225°C to improve separation and resolution, by holding at 50°C for 4 minutes initially, heating to 120°C at

20°C min^{-1}, holding for 10 seconds, heating to 180°C at 2°C min^{-1}, holding for 10 seconds and finally heating to 225°C at 4°C min^{-1} and holding for 40 minutes. Helium at 1.0 ml min^{-1} was used as a carrier gas. An internal standard (C13:0) and a mixture of external methyl ester standards of expected fatty acid composition of the sample (Sigma Aldrich, Gillingham, UK) were used for identification and recovery efficiency purposes.

Using the output from the GC the proportion of fatty acids was initially calculated as a percentage of the total fatty acid present (g fatty acid / 100g of total fatty acid). The values were expressed as percentage of total fat using a correction factor from Paul and Southgate (1976). The fatty acid content on a fresh muscle tissue basis (mg fatty acid / g of muscle tissue) was calculated using the intramuscular fat content of the sample. The main fatty acid groups such as SFA, MUFA, PUFA, CLA and *trans* were calculated (see Appendix 4).

3.6 Warner-Bratzler Shear force

Slices of LD 25 mm thick in polythene bags were placed in a water bath at 75°C and cooked for 50 minutes. Following cooking the bags were placed in ice slush, cooled for a minimum of 30 minutes, then removed and stored at 2°C overnight prior to performing the shear test. Cores of meat, 12.5 mm in diameter, were removed from the steaks in the direction of the muscle fibre. 10 cores were assessed from each loin with each core being sheared across the fibre direction by the WBSF attachment. The Warner-Bratzler shear test was performed using an Instron Universal Testing Machine (Instron Model 3366 Universal Testing Instrument) fitted with an inverted V shaped blade.

3.7 Statistical analysis

Principal component analysis of the fatty acid data was undertaken using Genstat V to identify whether there were any outliers in the dataset. The relationship between acceptability and WBSF values was evaluated using two different approaches: the first used individual responses to derive the model, whereas the second approach followed that of Platter *et al.* (2003) where an acceptable decision was based on 2/3 acceptable responses. The first approach used a generalized linear mixed model with acceptability as the dependent variable, WBSF as a fixed effect, and animal and panellist as random effects in the analysis. The model employed used a binomial distribution with a logit link function. After analysis the probability of acceptance, together with 95% confidence interval, was calculated for representative values of WBSF. Each piece of meat was tasted by 10 panellists; thus in the second approach a piece of meat was deemed to be acceptable if 66% or more of people found it acceptable (this approach was that used by Platter *et al.*(2003)). The analysis used a generalized linear model with binomial distribution and logit link function. Predictions and 95% confidence intervals were calculated as above.

Unscrambler (v9.8, Camo, Norway) multivariate software was used to build prediction models for Raman spectroscopy using the partial least squares (PLS) routine. The initial calibration models were evaluated for outliers using Hotelling's T2 test (strong outliers) and distance to model (weak outliers), using a 95% confidence interval. Any spectra which

were outliers were invariably found to be outliers due to signal noise, and these signals were removed from the dataset and the model rerun.

Hyperspectral NIR images were analysed using ENVI 4.4 and IDL 6.4 (ITT Visual Information Solutions) to determine mean spectra for identified regions of each sample. These spectra were imported into WinISI v1.02 software (Foss NIRSystems, Infrasoft International, LLC) for development of predictions for the reference quality attributes.

Prior to calibration development, spectral data were transformed by two methods: scatter correction and derivatives. Scatter correction is used to minimize the non-linear effect of light scatter due to particle size differences among samples (Barnes *et al.*, 1993). The imported mean spectra were treated using different methods of scatter correction: Standard Normal Variate (SNV) or De-trending (DT), or a combination of both SNV and DT. The spectra were also converted to different orders of derivative - i.e. first or second derivatives - to accentuate subtle differences. The NIR calibrations were then developed using partial least squares (PLS) regression in which samples from the calibration set were successively removed and predicted using remaining samples. This was used to aid in selection of the most appropriate factors to be included as well as to give a more robust determination of error.

To avoid the risk of over-fitting, usual guidance is to use a maximum of (n-10)/10 factors for n samples, and the maximum limit of 16 factors was used. Two parameters, coefficient of determination (R^2) and standard error of cross validation (SECV), were used to describe the fitness of models generated. SECV is based on the combined performance of the predictions of each of the groups removed in succession and as such gives a more realistic assessment of future calibration performance (Millar and Hall, 2004).

4 Results

4.1 Carcasses & Meat Quality

The distribution of conformation and fat class for all carcasses selected is shown in Table 1. The distribution of ultimate pH (pHu) values for the three sex types is shown in Figure 2(a), (b) and (c). A number of animals had high pHu values and therefore were not considered for consumer evaluation. All samples with pHu $\geq$ 5.8 were removed from consumer evaluation and were not used for the development of prediction equations for hyperspectral imaging or Raman spectroscopy. The range of carcasses and meat quality parameters for those animals used for the predictor models (i.e. pHu < 5.8) are given in Table 2.

Table 1 - Distribution of conformation and fat class for all carcasses selected

	Conformation Score							
Fat Class	E	U	R	O+	O	O-	Total	%
2	4	9	13	1	0	1	28	*17.1*
3	2	26	54	14	3	3	102	*62.2*
4L	0	7	15	2	0	0	24	*14.6*
4H	0	3	5	1	0	0	9	*5.5*
5	0	0	0	1	0	0	1	*0.6*
Total	6	45	87	19	3	4	164	
%	*3.7*	*27.4*	*53.0*	*11.6*	*1.8*	*2.4*		

Figure 2 – Distribution of ultimate pH values for the three sex types

(a) Bull pHu

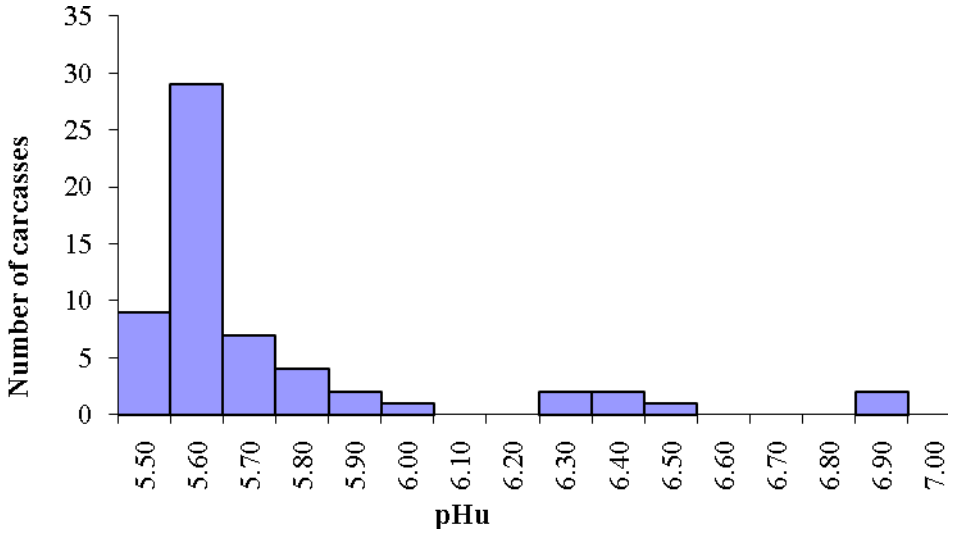

(b) Heifer pHu

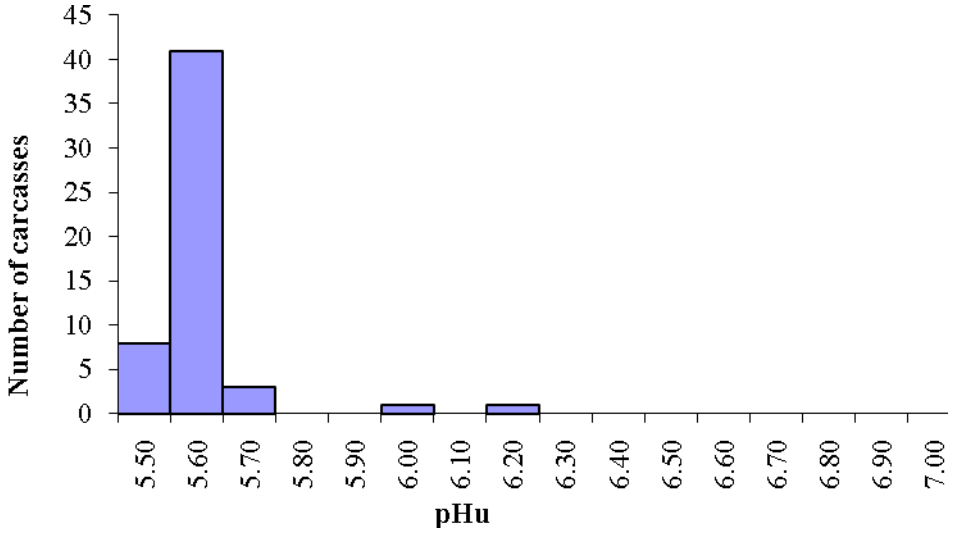

(c) Steer pHu

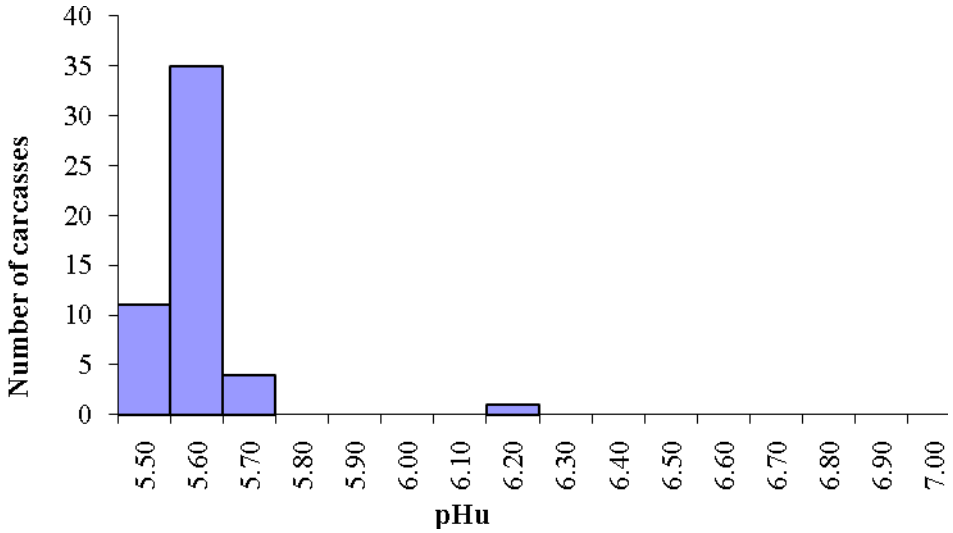

Table 2 - Summary of carcasses and meat quality parameters

	n	Mean	SD	Min.	Max.
HSCW (kg)	150	369.5	53.7	247.4	530.6
MSA Marbling Score[a]	150	346.5	76.6	140.0	540.0
pH Probe	150	5.6	0.1	5.5	5.8
Cooking Loss Day 14 (%)	150	26.5	3.2	20.2	54.6
WBSF Day 14 (kg)	150	5.2	1.3	3.1	10.1
Cooking Loss Day 21 (%)	150	29.2	2.3	23.4	34.8
WBSF Day 21 (kg)	150	5.1	1.1	2.8	9.9

[a] *Subjective assessment based on Meat Standards Australia Marbling procedures; n: number of observations; SD: standard deviation; Min: minimum value; Max: maximum value.*
HSCW: hot standard carcass weight
WBSF: Warner-Bratzler shear force

The initial selection of carcasses for the experiment resulted in a number of carcasses, mainly bulls, with high ultimate pH values. Those high pHu samples were not considered suitable for consumer evaluation; therefore, additional carcasses were collected to obtain the target of 150 for prediction purposes. Information on the total carcasses selected is given in Appendix 1. Only the carcasses with pHu less than 5.8 were used for prediction purposes.

A summary of conformation and fat class for the carcasses used for the prediction (pHu < 5.8) is given in Table 1. The distribution of carcasses selected in the current study had a greater percentage of better conformation grades E and U compared to MLC statistics for GB in 2008 (MLC 2008, E 0.3%, U 14.1%) and a lower percentage of O and P grades (MLC 2008, O 39.8%, P 2.0%). In the current study there was a greater percentage of carcasses in the lower fat class categories than in the MLC distribution for prime beef in 2008. The meat quality data are summarised in Table 2 (a breakdown by sex type is given in Table 11, Appendix 1) and the distribution of WBSF values are shown in Figure 26 in Appendix 1.

4.1.1 Fatty acids

The mean and range of fatty acids measured is given in Table 3. This table shows that there was a wide range of fatty acids measured in the meat samples collected.

Principal components analysis showed that 54% of the variation in the data could be accounted for by 3 principal components (PC1: 29.5%, PC2: 14.1% and PC3: 9.2%). In Figure 3, the majority of the bulls are positioned in the lower half of the PC plot with negative PC2 scores and also tend towards the left of the diagram with low to negative PC1 scores. These sex differences may represent different husbandry conditions, especially diet, as it might be expected that bulls would be finished under housed conditions receiving a predominantly cereal-based diet and are unlikely to be finished on grass. This is supported by the loadings plot in Figure 4 where those fatty acids which would be associated with mainly grass-based diets, are found to be positioned in the similar area on the PCA plot (i.e. upper half) as the heifers and steers. These include the principle fatty acid in grass lipid, C18:3*n*-3, an elongation product of this acid, C22:6*n*-3, as well as biohydrogenation intermediates such as the *trans* fatty acid C18:1*t*11. Those fatty acids positioned in the lower left quadrant such as the omega-6 (n-6) fatty acids C18:2*c*9,12 and its elongation product C20:4*n*-6, as well as a biohydrogenation intermediate C18:1*t*9, would be expected to be higher in the tissue of cattle finished on concentrates rather than grass (Alfaia *et al.* 2009).

Table 3 - Summary of fatty acid profiles in muscle tissue (mg fatty acid / g muscle tissue)

	Mean	SD	Min.	Max.
Intramuscular fat (g / 100g)	2.98	1.53	0.80	7.92
Fatty acid (mg / g muscle)				
C10:0	0.00	0.01	0.00	0.04
C12:0	0.01	0.02	0.00	0.18
C13:0	0.29	0.14	0.09	1.05
C14:0	0.71	0.43	0.11	2.18
C14:1*c*9	0.05	0.04	0.00	0.29
C15:0	0.13	0.09	0.00	0.42
C15:1*c*	0.13	0.08	0.00	0.58
C16:0	6.93	3.69	1.62	18.93
C16:1*t*9	0.07	0.05	0.00	0.34
C16:1*c*9	0.86	0.48	0.14	2.31
C17:0	0.30	0.17	0.06	0.96
C17:1*c*	0.21	0.12	0.04	0.70
C18:0	4.63	2.53	1.13	13.97
C18:1*t*9	0.09	0.12	0.00	0.83
C18:1*t*11	0.77	0.58	0.06	4.00
C18:1*c*9	9.84	5.46	1.82	27.80
C18:1*c*11	0.36	0.17	0.15	1.02
C18:2*t*9,*t*12	0.13	0.08	0.00	0.38
C18:2*c*9,*c*12	0.98	0.57	0.40	5.55
C18:3*n*3	0.25	0.12	0.08	0.75
CLA*c*9,*t*11	0.16	0.10	0.03	0.62
CLA*t*10,*c*12	0.18	0.11	0.02	1.09
C20:4*n*6	0.11	0.08	0.00	0.40
C20:5*n*3	0.02	0.04	0.00	0.21
C22:5*n*3	0.11	0.05	0.00	0.36
C22:6*n*3	0.00	0.01	0.00	0.04
Fatty acid groups (mg / g muscle)				
SFA	13.01	6.83	3.23	34.17
MUFA	11.46	6.29	2.16	31.31
PUFA	1.49	0.62	0.69	6.44
trans	1.41	0.80	0.30	4.79
CLA	0.34	0.17	0.06	1.45

SFA: saturated fatty acids; MUFA: monounsaturated fatty acids; PUFA: poly unsaturated fatty acids; trans: trans fatty acids; CLA: conjugated linoleic acid

Figure 3 – Scores plot for fatty acid composition principal components

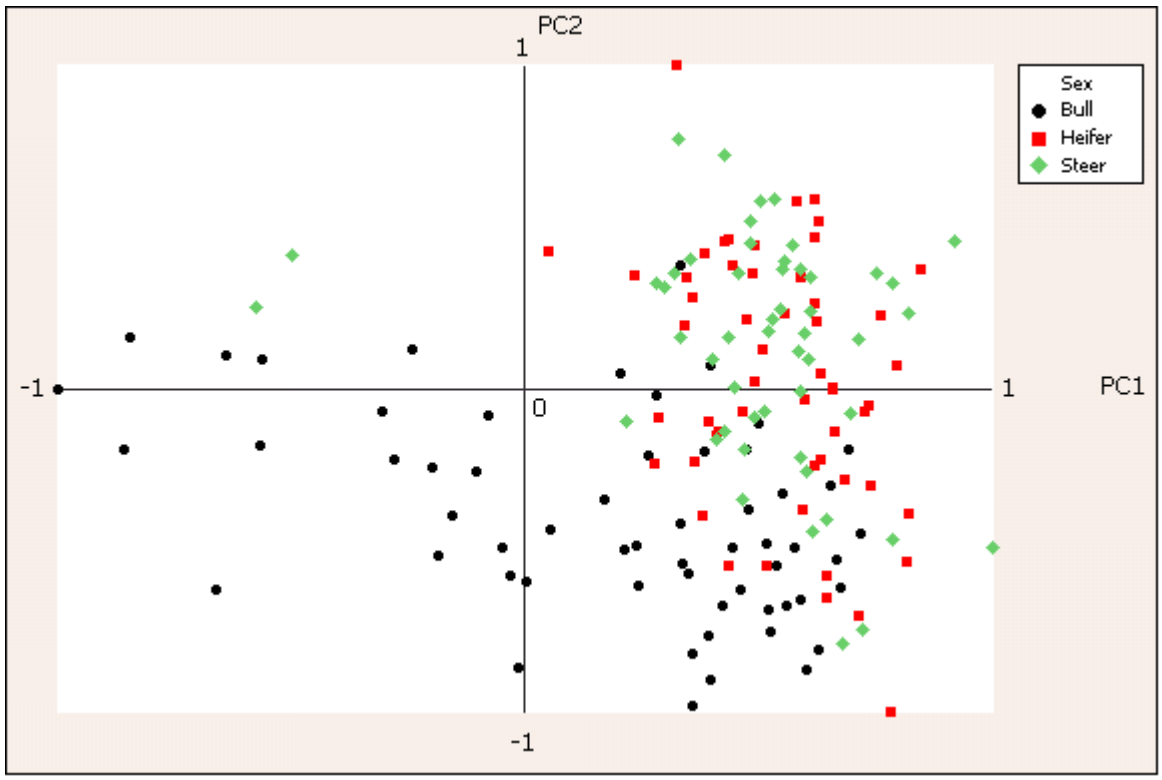

Figure 4 – Loadings plot for principal components of fatty acids

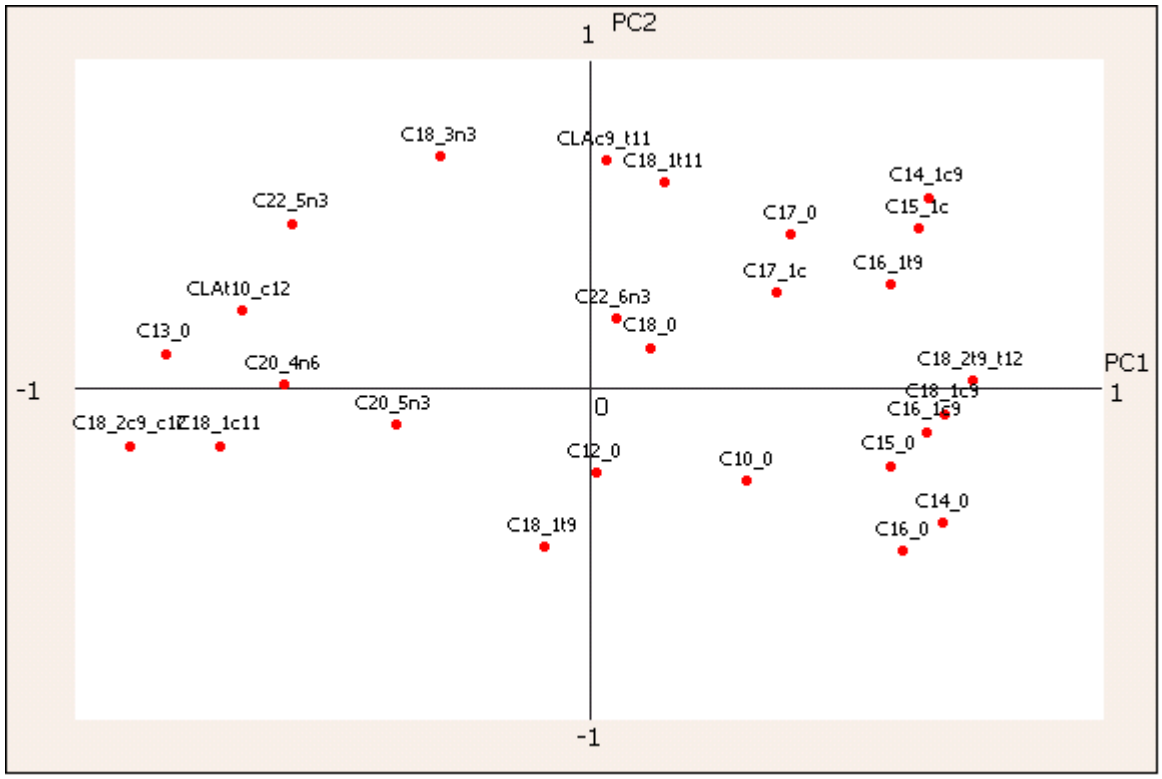

4.2 Consumer evaluation

The LD samples from each carcass were evaluated by 10 consumers; the average for each carcass at the appropriate aging time was calculated for development of the prediction models. Table 4 shows the summary statistics based on average results of the 10 consumers for each sample. It should be noted that when the data for individual consumers are examined there is a wide range of individual scores using the whole length of the 100 point line scale. The consumer data have not been clipped to remove these extreme scores (0 and 100). Table 4 shows that for each attribute there is a wide range of consumer scores.

Table 4 - Summary of consumer scores for sirloin aged 14 days

	Days aged	n	Mean	SD	Min.	Max.
Tenderness_Score	14	144	50.5	14.25	8.40	80.68
Juiciness_Score	14	144	48.88	12.06	19.02	74.63
Flavour_Score	14	144	52.26	10.72	24.49	75.05
Overall_Liking	14	144	50.97	11.73	16.98	77.19
CMQ4_Score	*14*	*144*	*50.82*	*12.18*	*16.00*	*77.65*

*CMQ4 score: combined meat quality score = 0.4*Tenderness + 0.1*juiciness + 0.2*flavour + 0.3*overall liking; n: number of observations; SD: standard deviation; Min.: minimum value; Max.: maximum value.*

4.3 NIR hyperspectral imaging

4.3.1 Image analysis

4.3.1.1 Calculation of reflectance

The hyperspectral data for each sample comprise a 3 dimensional data cube comprising spectra for each pixel in the image, with 240 spectral bands spanning a wavelength range of 993 to 2495 nm. To calculate reflectance spectra, the mean dark reference image recorded at the end of each scan was subtracted from the data for each scan line and the data were then normalised by the baseline-corrected data for the white reference sample to correct for the spectral response of the detector, the illumination spectrum, the spatial distribution of the illumination and the sensitivity of each detector pixel.

4.3.1.2 Classification of lean and fat

The data were first analysed to calculate the reflectance at 1081 nm, as exemplified in Figure 5(b). A colour image of the same sample is shown in Figure 5(a) for reference. The sample was discriminated from the background by selecting the pixels with greatest reflectance at this wavelength according to the criterion

$$R_{1081} > 0.2 \quad (1)$$

or equivalently

$$\log(1/R_{1081}) < 0.7 \quad (2)$$

The largest identified region was selected and any holes filled (Figure 5(c)).

Figure 5 – Identification of sample regions

(a) Colour image

(b) NIR reflectance at 1081nm

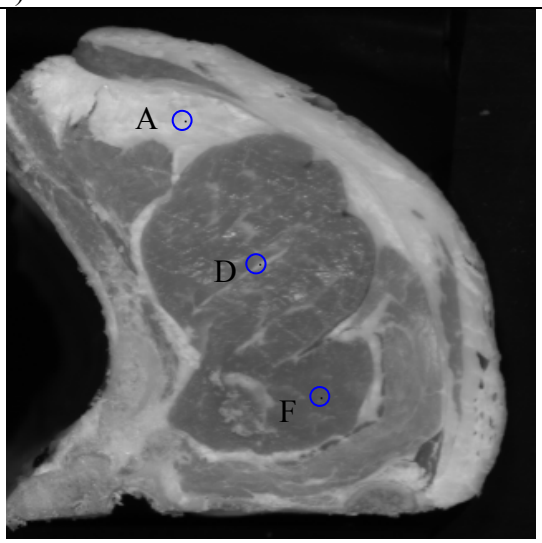

(c) Identified region of sample, R_{1081}>0.2

(d) Area of absorbance band between 1647 and 1743 nm

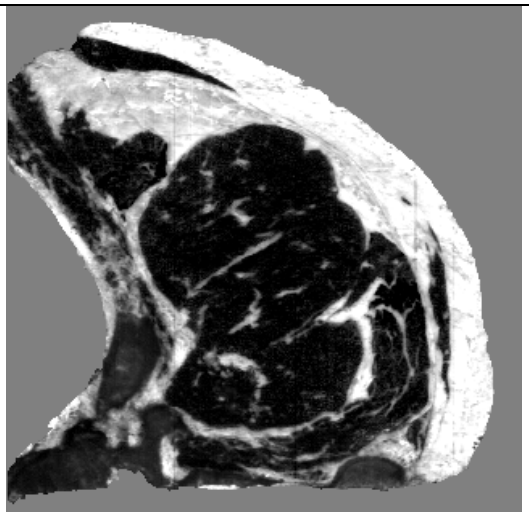

(e) Classification of lean and fat.

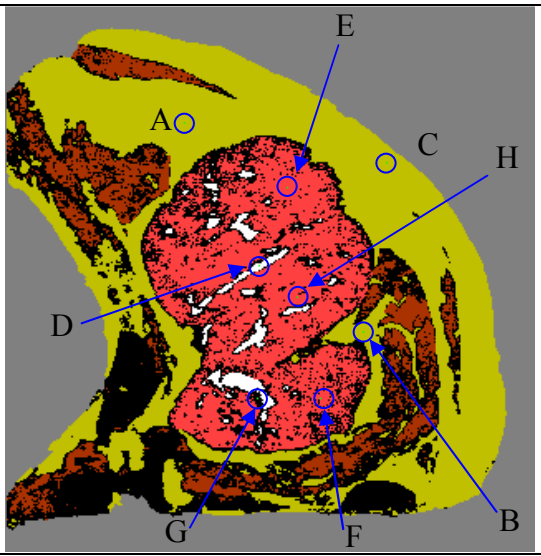

(f) Regions of high specular reflection (red) overlaid on fat distribution.

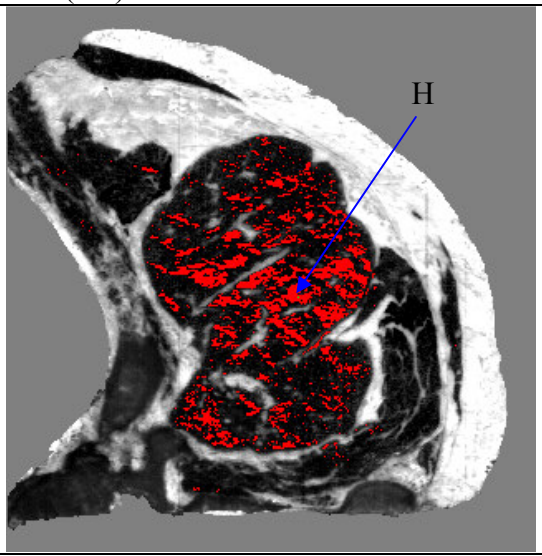

Figure 6 – Example spectra

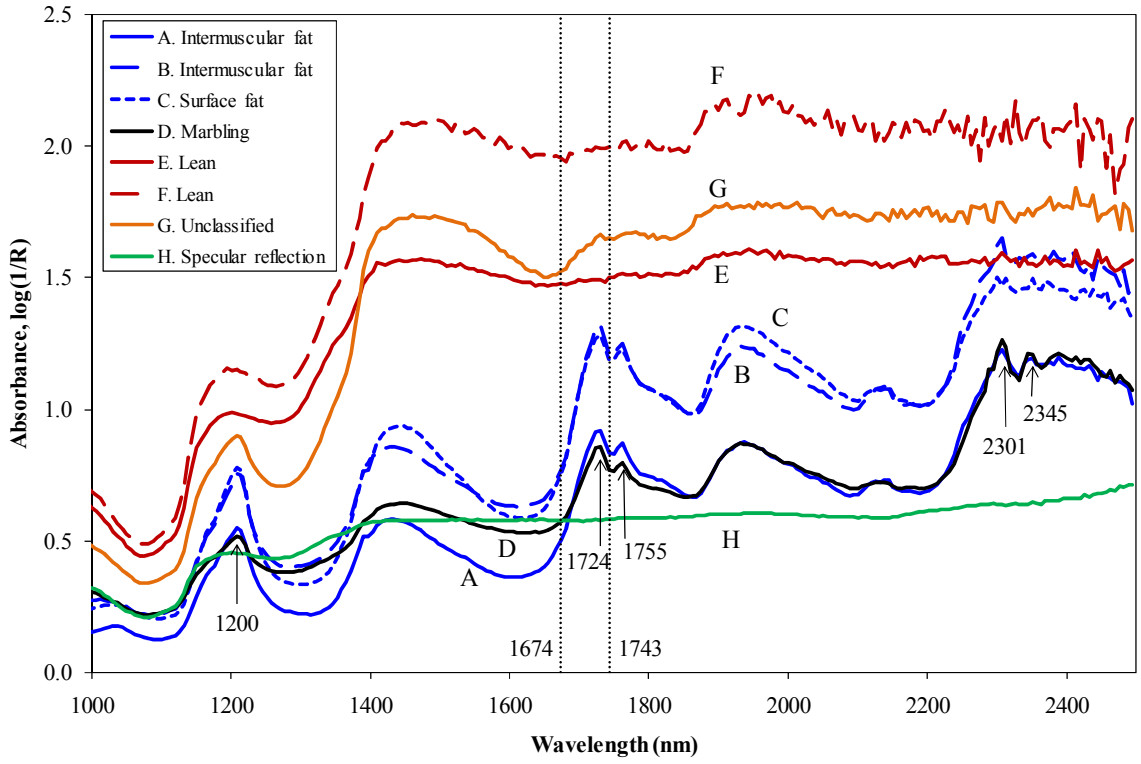

Figure 6 shows example spectra for several pixels in the example image. The spectra labelled A, D and F correspond to regions of intermuscular fat, marbling fat and lean muscle respectively, at the positions indicated in Figure 5 (b).

The major NIR absorption bands in fat are a CH_2 2nd overtone at 1200nm, CH_2 1st overtones at 1734 and 1765 nm and CH_2 stretch-bend combinations at 2310 and 2345 nm (Osborne *et al.*, 1993). These are indicated in Figure 6, with measured peak wavelengths of 1200, 1724, 1755, 2301 and 2345 nm respectively, to within the band spacing of 6 nm.

Multivariate methods are available to classify spectra based on the statistics of populations of known reference samples of each class. To classify pixels as lean or fat by such methods would require reference spectra for pixels known to represent either lean or fat, measured under similar conditions to those used. In practice, no independent data were available upon which to base such a classification. Pixels were instead classified based on the strength of the CH_2 absorbance band at 1724 nm. It can be seen from Figure 6 that this is present in the spectra A and D for regions of fat, but absent from the spectrum F of a lean region. The strength of the 1724 nm band was determined by measuring the area, *A*, under the absorbance spectrum between the wavelengths 1674 and 1743 nm (indicated by vertical dashed lines in Figure 6), measured relative to a straight baseline between the absorbances at these wavelengths. Figure 5(d) shows the distribution of this band area within a sample, with brighter shading representing a greater band area. Of several potential classification methods based on the area or 2nd derivative of the fat absorption bands, or on the reflectance of the sample, it was considered that this gave the best correspondence with the visible locations of marbling fat in the reference colour images, and there is a good correspondence between the

bright regions in Figure 5(d) and the visible regions of fat in Figure 5(a). It should be noted that the classification by NIR correctly discriminates fat from bone, which is less easily distinguished in colour images (e.g. region J in Figure 5(a)).

Pixels were classified according to the following criteria:

$$\begin{aligned} A &> 0.5 \quad \text{Fat} \\ A &< 0.1 \quad \text{Lean} \end{aligned} \tag{3}$$

Pixels with intermediate band area could not be reliably identified as lean or fat and may, in some cases, correspond to combined lean and fat spectra, and were therefore not classified. Figure 5(e) shows an example of the classification result with fat shown in yellow and white, lean shown in red and unclassified pixels shown in black.

Figure 6 shows example spectra for several positions indicated in Figure 5(e), including examples of intermuscular fat (A, B), surface fat (C), marbling fat (D) and lean muscle (E, F). G shows an example of an unclassified pixel for which the band area was intermediate between the criteria for lean and fat. It can be seen that pixels at the boundary of marbling fat were often unclassified. It is likely that pixels in such positions include a contribution from both the adjacent lean and fat regions, resulting in an intermediate spectrum.

Some pixels, such as that marked as H, had a relatively flat spectrum with few resolvable bands and typically a high reflectance. This is caused by specular reflection of the light source from the sample surface. An attempt was made to identify pixels with high degrees of specular reflection according to the criterion:

$$R_{1938} - R_{1624} < 0.1 \tag{4}$$

Pixels identified by this criterion were excluded from use in calibrations. Figure 5(f) shows the pixels identified by this criterion, superimposed on the fat distribution image. It can be seen that specular reflection was mainly confined to the lean regions of the sample.

4.3.1.3 Delineation of regions of interest

Images were taken for the whole cut surface of the forerib. However, for this work, only regions corresponding to the LD muscle were required for development of predictions. Although it might, in principle, be possible to identify the position of this muscle automatically by analysis of the images, development of such a method was beyond the scope of the project and it was considered more practical to delineate the position of the required muscle manually. To facilitate this, the images were first analysed to determine the position of the sample and the classification of lean and fat regions as described above. A false colour bitmap image was saved for each sample, identifying these classifications. Each image was then annotated manually to mark the border of the LD muscle. The position of the region of intermuscular fat indicated as A in Figure 5 was also marked for potential use as an alternative to marbling fat in case there were insufficient marbled samples for this purpose; in practice there were sufficient marbled samples and the intermuscular fat was not used in the analysis. The data were then reanalysed. The regions of lean and fat were classified as

before. Pixels lying within the area identified as the LD were considered. Any regions of fat lying at the edge of this region were considered to represent intermuscular, rather than marbling fat and were excluded from consideration. All other pixels within the identified region were used for calculation of mean spectra and are identified as bright red and white regions in Figure 5(e).

4.3.1.4 Calculation of mean spectra and output of data

Within the LD region, the following spectra were calculated:

- Mean spectrum for all non-specular pixels
- Mean spectrum for all non-specular pixels classified as fat
- Mean spectrum for all non-specular pixels classified as lean

The mean spectrum was also calculated for the non-specular pixels of intermuscular fat lying within a 15 pixel (≡ 9.4 mm) radius of the identified position corresponding to position A. However, this was not required for subsequent analysis.

During calculation of each mean spectrum, consideration was given to bands or pixels for which the raw data were saturated, preventing calculation of a reliable reflectance value. For each band, if fewer than 10% of the pixels under consideration were saturated, these pixels were excluded from calculation of the mean spectrum. If more than 10% of the pixels for a particular band were saturated, the band was instead marked as bad in the output mean spectrum.

The numbers of pixels in the following categories were also calculated.

- Area of sample (corresponding to the filled area in Figure 5(c), subdivided into:
    - Area classified as fat (yellow + white in Figure 5(e))
    - Area classified as lean (light + dark red in Figure 5(e))
    - Area not classified (black in Figure 5(e))
- Intermuscular fat region centred on A
- Area of LD muscle, subdivided into:
    - Marbling fat (white in Figure 5(e))
    - Lean (bright red in Figure 5(e))
    - Unclassified
- Intermuscular fat region A, excluding specular reflections
- Area of LD muscle, excluding specular reflections, including
    - Marbling fat
    - Lean
- Number of pixels included in LD mean spectrum, excluding saturated data.
- Number of pixels included in LD marbling fat mean spectrum, excluding saturated data.
- Number of pixels included in LD lean mean spectrum, excluding saturated data.

Spectra were saved for import into WinISI for calculation of predictions.

4.3.2 Blooming effects

Scans and digital images of each sample were made for a freshly cut surface and for the same surface after storage of the sample at 2°C for at least an hour, allowing the sample to bloom.

Figure 7 – Cut surface appearance before and after blooming

Unbloomed	Bloomed
	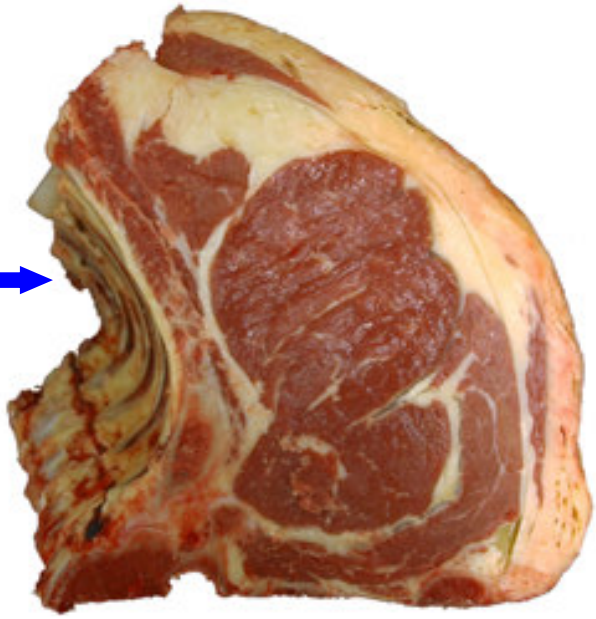
	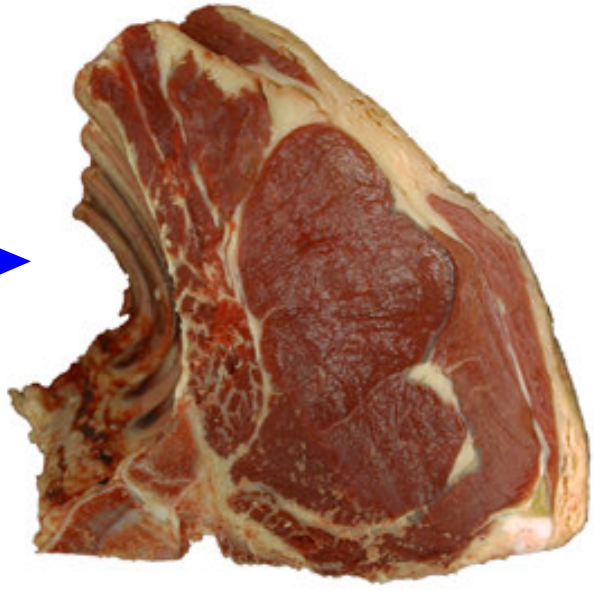

Figure 8 – Spectral differences of blooming effect for each region of beef

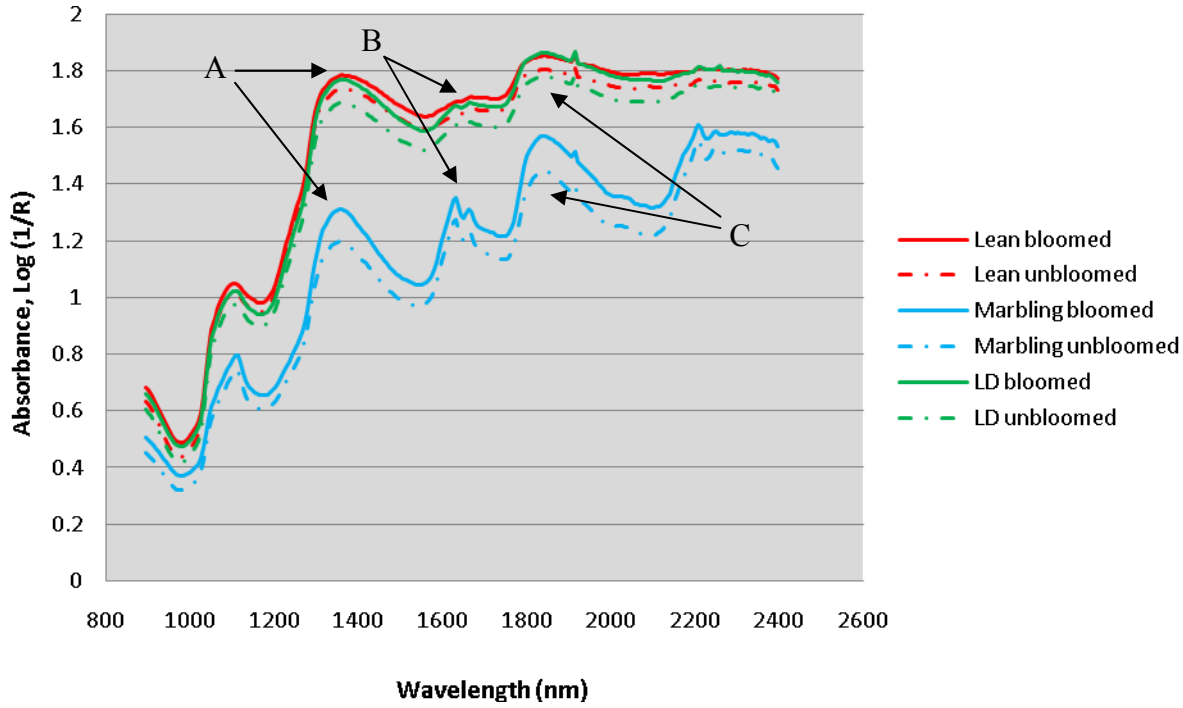

Figure 7 shows the colour changes of the cut surfaces before and after blooming. The images have been adjusted using the colour reference card to compensate for variations in imaging conditions during the experiments. The colour of the lean region on the freshly cut surface changed from dull red to bright red after blooming, due to oxygenation of myoglobin to oxymyoglobin, which is bright red in colour. Figure 8 shows a comparison between the NIR spectra of a sample before and after blooming for the indentified regions of forerib. Bloomed samples had overall stronger absorbance than unbloomed samples, particularly for marbling fat regions. The fat absorbance is present as a doublet peak (B) at 1624 nm and 1655 nm. Lean and total LD spectra have similar patterns over the full measured wavelength range, with a stronger contribution of band B in the latter due to the inclusion of marbling fat. There are no major differences in the other significant absorbance bands, A and C, before and after blooming.

4.3.3 Prediction models

Mean spectra were calculated for the total area of the LD (total LD) which includes a contribution from marbling fat within the LD. These mean total LD spectra were used to develop prediction models for WBSF, eating quality, percent intramuscular fat (g / 100g) and major fatty acid groupings (SFA, MUFA, PUFA & CLA) expressed as mg/g muscle tissue. The mean spectra LD (LD Lean) which excluded marbling fat (see Section 4.3.1.4) were used to develop prediction models for WBSF and eating quality (note: as this did not contain information from regions of marbling it was not considered relevant to predict fatty acid profiles from these mean spectra) The mean spectra obtained from the marbling fat within the LD were used to predict major fatty groupings (SFA, MUFA, PUFA & CLA) expressed as g / 100g fat. The resulting mean spectra were pre-treated with scatter correction and were converted into different orders of derivatives for further calibration development.

PLS regression with full cross validation was used to determine any correlation between the spectral data for the identified regions and the reference measurements with respect to texture, sensory and fatty acids. Several calibration methods were assessed. Table 5 shows the best performance of the parameter standard error of cross validation (SECV) and the relevant coefficient of determination (R^2) describing the fitness of the models for each region and predicted property.

In terms of R^2, models based on spectra from bloomed samples gave the best overall performance. The results of calibration parameters for texture and sensory assessments obtained with spectra from the lean and total regions of the LD are about 0.5, indicating a negligible effect of the inclusion of marbling fat in the spectra for the latter. Calibrations based on average spectra for the whole muscle surface showed a fairly strong correlation ($R^2 = 0.7$) with fat content. Measurements of total muscle also showed correlations with fatty acid content. It is possible that this may be due to variations in total fat content. However, calibrations based on fat spectra alone also showed correlations with some of the fatty acids, with similar performance for PUFA and CLA providing possible evidence for differentiation of fatty acids, although the prediction was poor for SFA. Despite this, an effect of total fat content may still be present for the predictions based on fat spectra, due to thinner marbling in samples of low fat content, which may result in partial inclusion of light from lean regions within the fat spectra from such samples. Figure 9 shows a scatter plot showing the best prediction of MUFA ($R^2 = 0.8$) based on the calibration achieved using unbloomed total LD spectra over the complete wavelength range.

Table 5 – Parameters describing the fitness of modelling the correlation between measurements and the reference data

		Spectral range (993 – 2495 nm)					
		All samples		Unbloomed		Bloomed	
Identified region	Variable predicted	R^2	SECV	R^2	SECV	R^2	SECV
Total LD	Force D14	0.46	0.74	0.46	0.76	0.61	0.75
	Tender D14	0.49	9.91	0.48	10.67	0.47	10.26
	Juicy D14	0.48	8.92	0.33	9.82	0.53	9.34
	Flavour D14	0.46	7.96	0.31	8.40	0.46	7.76
	O/all like D14	0.45	8.78	0.29	9.16	0.44	8.75
	Force D21	0.42	0.66	0.45	0.68	0.49	0.63
	SFA (mg / g muscle)	0.68	3.27	0.67	3.18	0.62	3.26
	MUFA (mg / g muscle)	0.75	2.86	0.80	2.84	0.71	2.90
	PUFA (mg / g muscle)	0.38	0.34	0.39	0.33	0.46	0.33
	CLA (mg / g muscle)	0.49	0.09	0.45	0.10	0.55	0.09
	% IMF (g / 100g fat)	0.73	0.71	0.74	0.72	0.70	0.73
LD lean	Force D14	0.56	0.71	0.55	0.77	0.61	0.73
	Tender D14	0.51	9.66	0.42	10.54	0.51	9.82
	Juicy D14	0.47	8.97	0.38	9.55	0.48	8.72
	Flavour D14	0.47	7.83	0.40	8.58	0.50	7.58
	O/all like D14	0.44	8.52	0.41	9.04	0.49	8.45
	Force D21	0.41	0.67	0.36	0.68	0.49	0.64
Marbling fat	SFA (g / 100g fat)	0.10	1.92	0.18	1.91	0.13	1.86
	MUFA (g / 100g fat)	0.39	2.12	0.19	2.22	0.43	2.13
	PUFA (g / 100g fat)	0.63	1.39	0.53	1.35	0.38	1.54
	CLA (g / 100g fat)	0.54	0.33	0.43	0.33	0.46	0.32

IMF intramuscular fat; SFA: saturated fatty acids; MUFA: monounsaturated cis fatty acids; PUFA: poly unsaturated cis fatty acids; CLA: conjugated linoleic acid

Figure 9 – Measured versus predicted MUFA (mg / g muscle) for unbloomed total LD over the complete wavelength range (993-2495 nm) for the hyperspectral imaging system

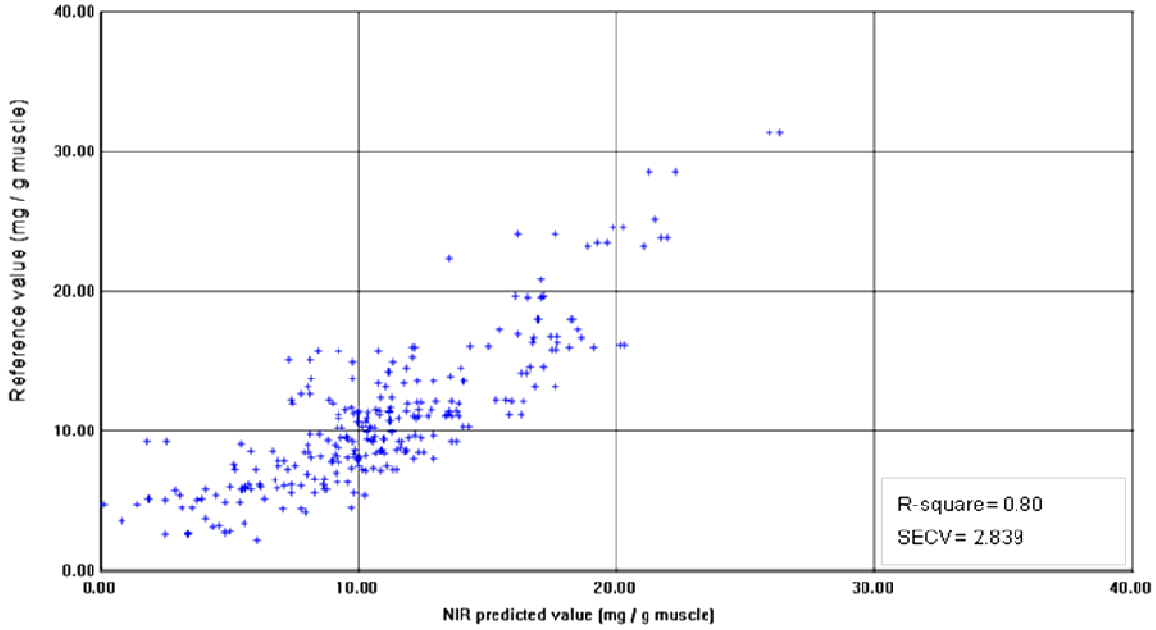

Figure 10 shows two samples with different areas of identified marbling fat. For the samples with large amounts of marbling fat present, such as Figure 10(a), relatively high confidence can be placed in the classification of most of the pixels identified as fat, and the resulting mean marbling spectra are based on a sample of a large number of fat pixels as shown in Figure 10(c). However, for samples with very little or no marbling fat present, as exemplified in Figure 10(b), relatively few pixels of fat are identified (e.g. 39 pixels in Figure 10(d)), providing greater sensitivity to factors such as noise, misclassified pixels, or pixels representing fat adhering to the meat surfaces due to the cutting operation. Fat spectra for such samples are also likely to include a greater contribution from neighbouring lean regions. Therefore, further predictions of fatty acid composition were developed, using only samples with the largest identified areas of marbling fat, and excluding samples with fewer than 50 identified marbling fat pixels.

Figure 10 – Identified marbling fat areas

(a) With marbling fat	(b) Little marbling fat
	
(c) Identified marbling fat area = 1025 pixels	(d) Identified marbling fat area = 39 pixels
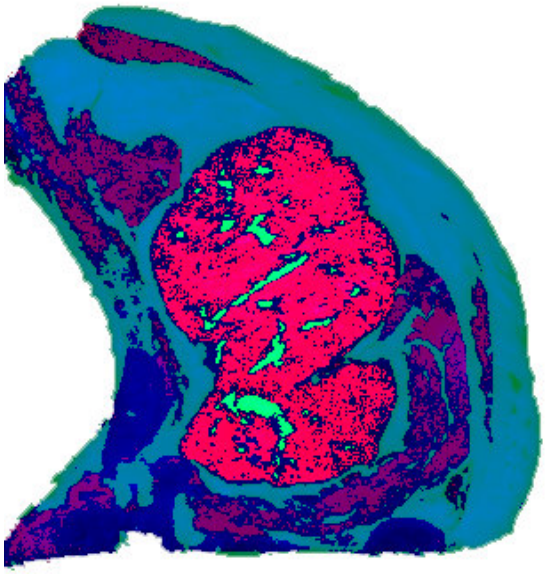	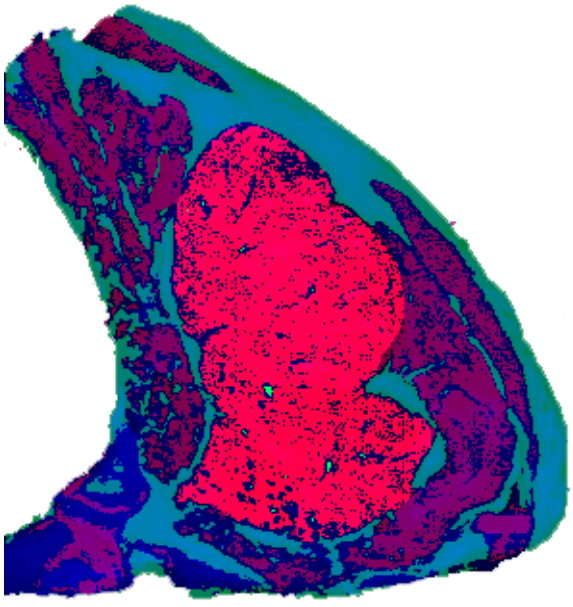

Table 6 shows the best performance of the parameters R^2 and SECV describing the fitness of the models based on marbling fat regions of (a) all samples and (b) samples with identified marbling fat area more than 50 pixels, against the reference fatty acids over the complete wavelength range. The overall results have been improved although such improvement is not shown in the prediction of PUFA. The model for prediction of SFA is particularly improved, with R^2 over 0.5, compared with previous R^2 of 0.1.

Figure 11 shows examples of scatter plots showing the measured SFA values versus the predicted SFA values based on calibration achieved in this way.

Table 6 - Parameters describing the fitness of modelling the correlation between measurements and the marbling fat reference data

(a) Whole range of samples

		Spectral range (993 – 2495 nm)					
		All samples		Unbloomed		Bloomed	
	Correlation	R^2	SECV	R^2	SECV	R^2	SECV
Marbling fat /	SFA (g / 100g fat)	0.10	1.92	0.18	1.91	0.13	1.86
	MUFA (g / 100g fat)	0.39	2.12	0.19	2.22	0.43	2.13
	PUFA (g / 100g fat)	0.63	1.39	0.53	1.35	0.38	1.54
	CLA (g / 100g fat)	0.54	0.33	0.43	0.33	0.46	0.32

(b) Samples with identified marbling fat area > 50 pixels

		All samples		Unbloomed		Bloomed	
	Correlation	R^2	SECV	R^2	SECV	R^2	SECV
Marbling fat /	SFA (g / 100g fat)	0.66	1.40	0.54	1.49	0.54	1.53
	MUFA (g / 100g fat)	0.58	1.60	0.46	1.79	0.56	1.68
	PUFA (g / 100g fat)	0.48	0.92	0.41	1.00	0.38	0.98
	CLA (g / 100g fat)	0.62	0.26	0.56	0.27	0.65	0.25

Figure 11 – Measured versus predicted SFA (g / 100 g fat) for unbloomed marbling fat over the complete wavelength range (993-2495 nm) for the hyperspectral imaging system

(a) Whole range of samples

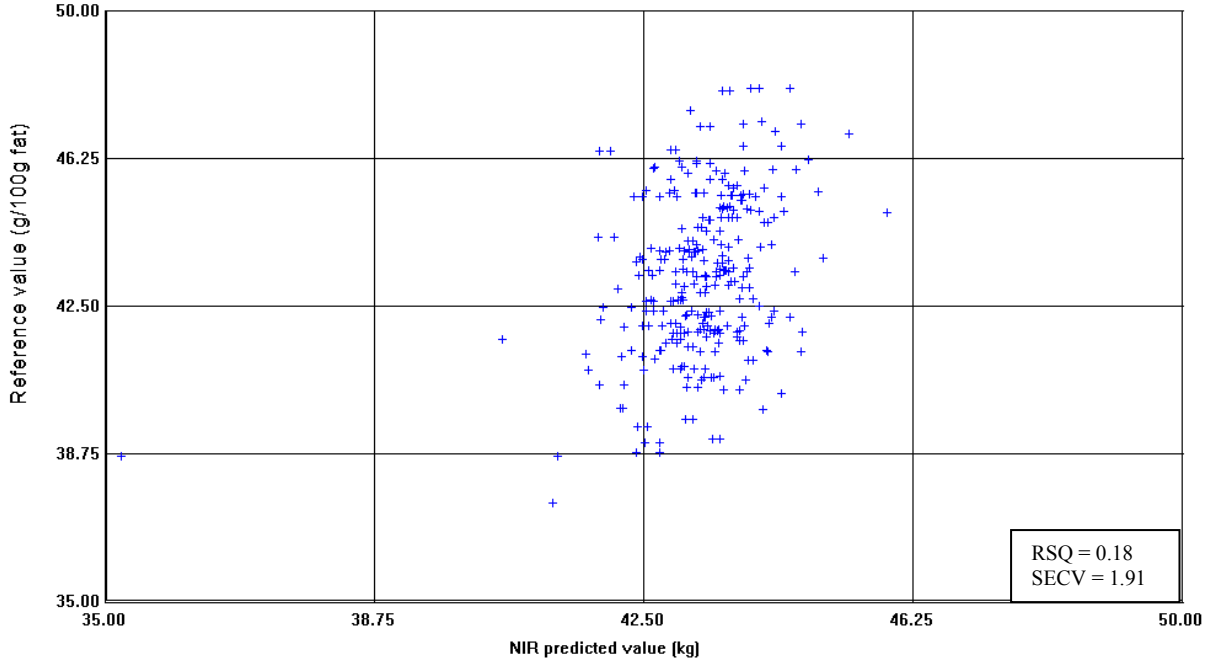

(b) Samples with identified marbling fat areas > 50 pixels

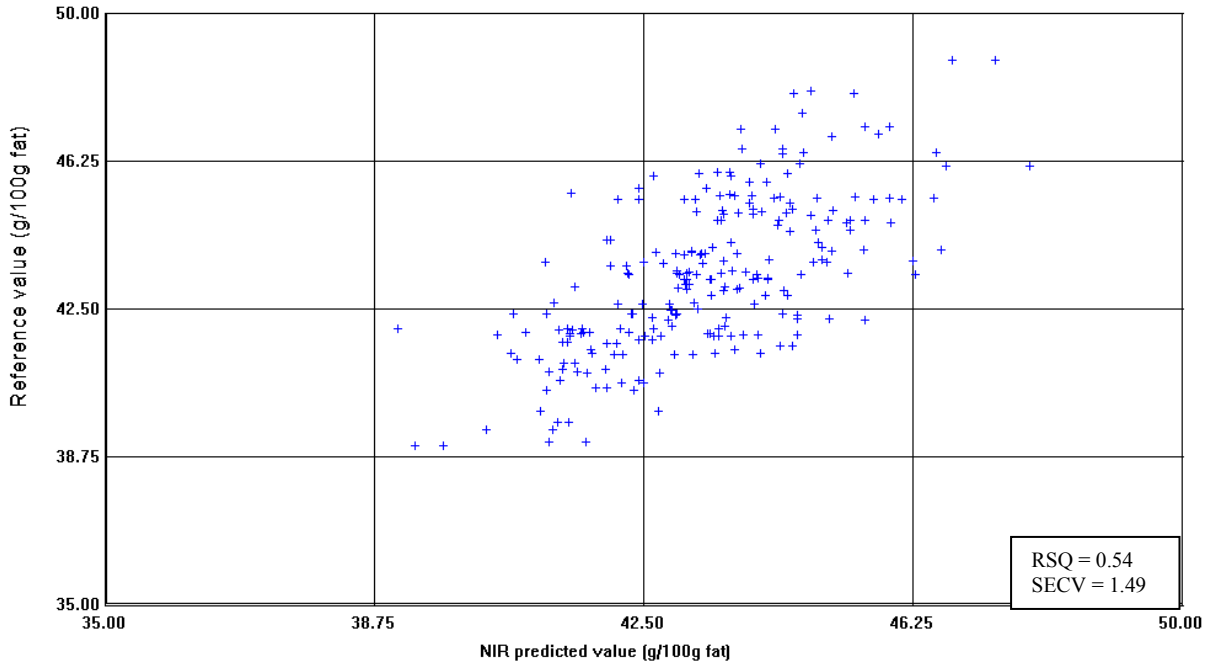

The hyperspectral approach developed in this project has clearly shown the potential to identify fat and lean regions of muscle surfaces, based on a CH_2 absorbance band at 1724nm. This classification may be able to be further refined by using more wavelengths and multivariate analysis (e.g. discriminant analysis). One of the objectives for identifying lean and fat separately was to determine the influence of marbling in the spectra on the prediction of shear force and eating quality. The results (Table 5) show that from both the coefficient of determination, R^2 and the standard error, SECV, the prediction of shear force and eating quality was similar when the total LD spectra (includes marbling fat contribution) or lean LD spectra (excludes marbling fat) were used to develop models.

Figure 12 and Figure 13 show the calibration coefficients used in the models for prediction of shear force and eating quality from the spectra of lean LD and total LD, respectively. Both figures show similarities in the wavelengths with the greatest weighting in the models. There are no particularly high coefficients over the wavelengths corresponding to any particular spectral peaks associated with shear force characteristics. However, there are a number of spectral bands which are associated with eating quality characteristics (peaks A to G). With the use of lean LD spectra in the prediction models for eating quality, the dominant peaks (A to G in Figure 12) corresponding to eating quality characteristics are generally situated in similar ranges of wavelengths as in the models obtained from total LD spectra (Figure 13), showing the effects of those particular wavelengths in the prediction models.

Figure 12 – Calibration coefficients used for the best predictions of shear force and eating quality obtained from lean LD spectra

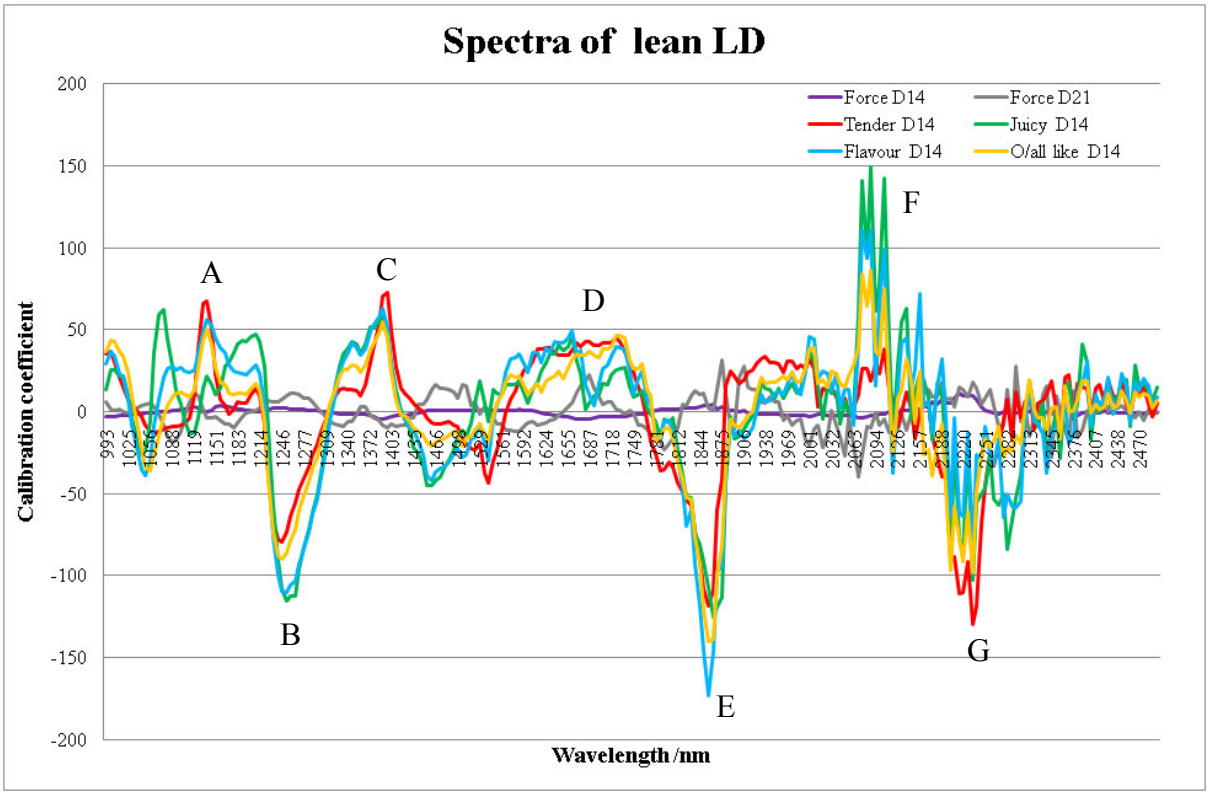

Figure 13 – Calibration coefficients used for the best predictions of shear force and eating quality obtained from total LD spectra

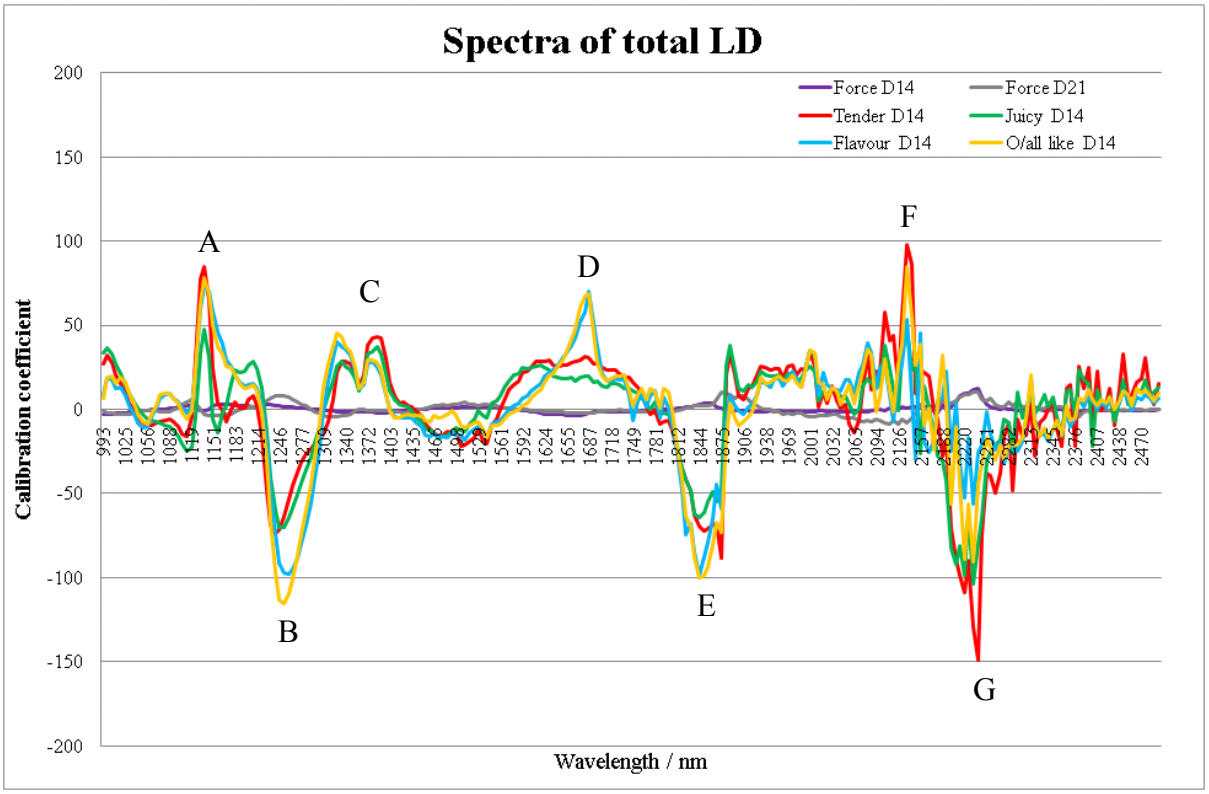

Prediction of fatty acid profiles using NIR measurements of muscle have been reported by other workers (Sierra *et al.*, 2008 & Realini *et al.,* 2004). In the published papers it is not clear whether some of the prediction ability may be due to the amount of intramuscular fat in the muscle and individual fatty acids are predicted since they show high correlations with intramuscular fat. The ability to identify marbling spectra in the current project allows a comparison of prediction based on total LD spectra (includes marbling fat) and spectra of marbling fat. Table 5 shows that the ability to predict the SFA and MUFA content in the muscle was high ($R^2 = 0.67$ and 0.80 respectively) when the total LD spectra were used but the ability to predict CLA and PUFA was lower ($R^2 = 0.55$ and 0.46 respectively). It is thought that these predictions may be due to the intramuscular fat content, which was also predicted with a high correlation coefficient ($R^2 = 0.73$). The proportion of saturated fatty acids increases as the intramuscular fat content increases (Warren *et al.* 2008).

Two approaches have been carried out to predict fatty acids by using the spectra of marbling fat: the inclusion of marbling fat spectra for all samples and the use of marbling fat spectra only for samples with identified marbling more than 50 pixels. The latter reduced factors such as noise, misclassified pixels and extra fat adhering to the meat surface, and improved the prediction models for fatty acids (see relevant prediction models in Table 6).

Removing samples with identified marbling fat less than 50 pixels improved the prediction models (Table 5 and Table 6). The errors of prediction models (SECV) for fatty acids (SFA, MUFA, PUFA and CLA) were largely improved as were the correlation coefficients;

however, the correlation coefficient of the prediction model for PUFA was slightly weakened. Although the diet of the cattle during the finishing period is not known it is likely that, in the current study, the random selection of animals resulted in cattle sourced from grass, concentrate and grass or silage /concentrate diets. Further evidence from this comes from the PCA, which indicates that the fatty acid profile of bulls is associated with concentrate based diets. To obtain reliable prediction of fatty acid profiles from cattle with a wide range of profiles, the wavelengths selected should be specific to the type of bond (e.g. C=C, C=O, chain length etc.). Although such spectral features can be easily identified in Raman spectroscopy (Beattie *et al*. 2007), NIR absorption bands are less well resolved and it is more difficult to assign measured absorbance bands to unique bonds.

Figure 14 and Figure 15 show the calibration coefficients used for fatty acid predictions obtained from marbling spectra (spectra of samples with identified marbling fat more than 50 pixels) and total LD spectra, respectively. There are no particularly high coefficients corresponding to particular spectral bands associated with SFA obtained from marbling spectra, whereas there is a clearer dependence of the model for total LD spectra on particular spectral regions. A clearer dependence of spectral regions associated with CLA is shown in the model obtained from marbling spectra. The coefficients corresponding to particular spectral regions associated with PUFA obtained from both spectra are in different ranges of wavelengths. Coefficients of several spectral regions (A to C, F to H) associated with MUFA show similarity in the range of wavelengths but are different in some spectral regions, e.g. D and E from marbling spectra, I and J from total LD spectra.

Figure 14 – Calibration coefficients used for the best predictions of fatty acids obtained from marbling fat spectra with identified fat area > 50 pixels

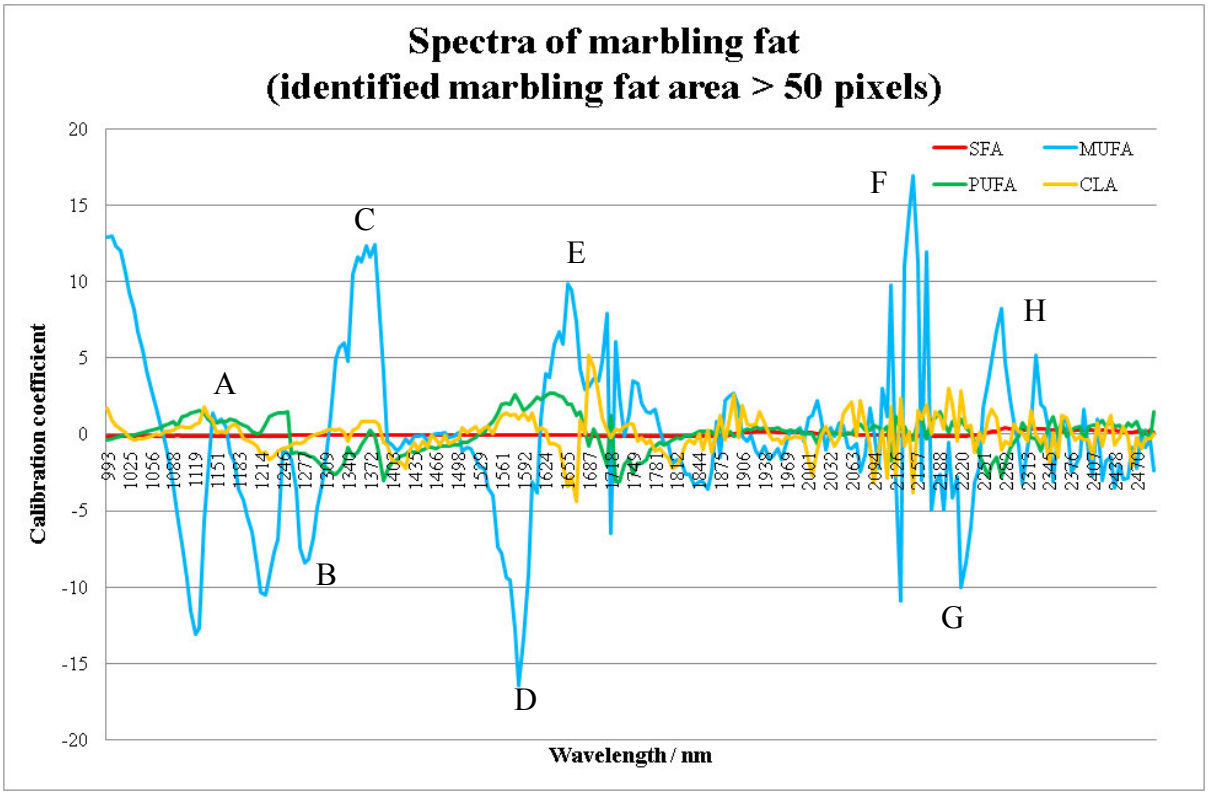

Figure 15 – Calibration coefficients used for the best predictions of fatty acids obtained from total LD spectra

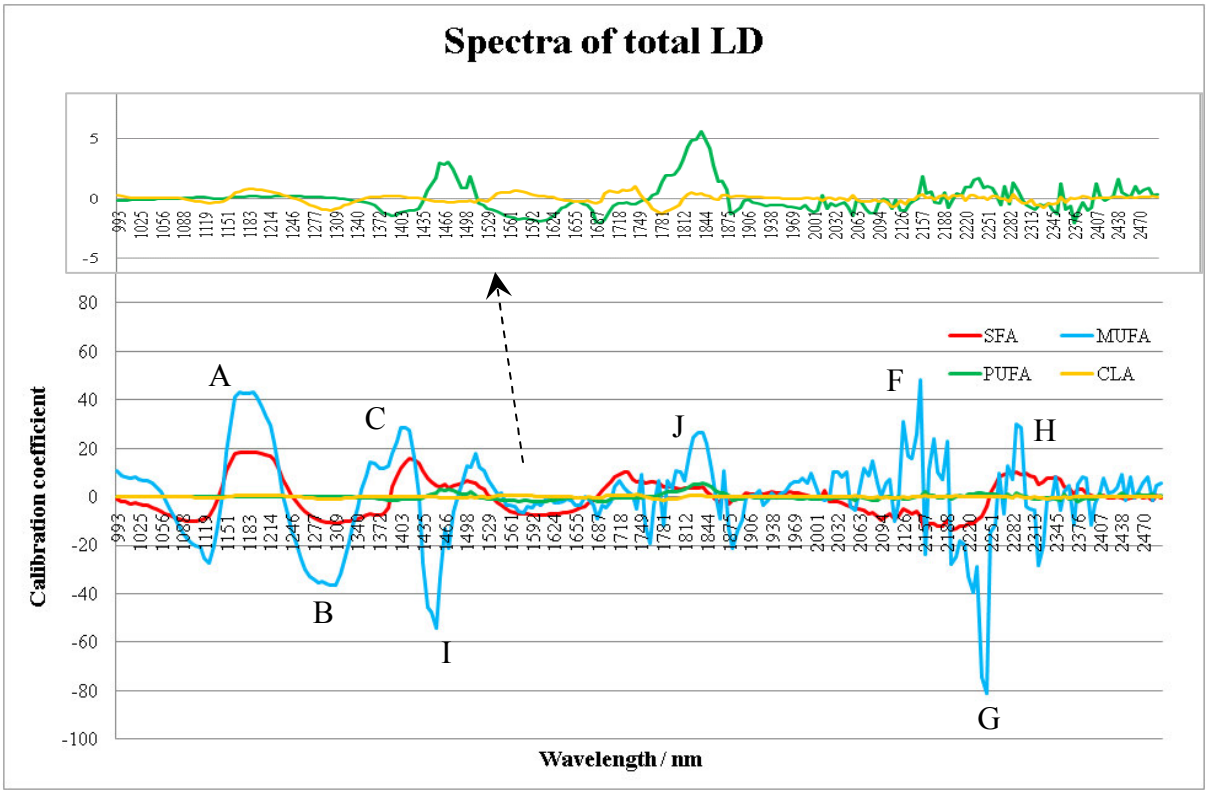

4.4 Raman Spectroscopy

Examples of Raman spectra obtained for the LD at 2 days post mortem are shown in Figure 16. In this figure the baseline of each spectrum has been offset for ease of comparison between them. Within each spectrum the magnitude of the Raman intensity is on the same scale. The spectra labelled b2 and b4 show spectral characteristics of protein i.e. the lean tissue. The spectrum labelled b3 shows typical characteristics of fat and is from a highly marbled sample. The spectrum labelled b5 shows a mixture of protein and fat characteristics. The spectrum labelled b1 shows a considerable amount of background noise (see Figure 27, Appendix 2 for comparison with published spectra). A number of spectra showed considerable noise and the reason for this has not been clearly identified, although the spectra were similar to the background optics signal, indicating possible problems related to focus for maximum signal (see Figure 27, Appendix 2). In developing the predictions the extreme noisy spectra were identified in the multivariate analysis and were not included in the model development.

Figure 16 – Example of Raman spectra of beef LD acquired 2 days post mortem

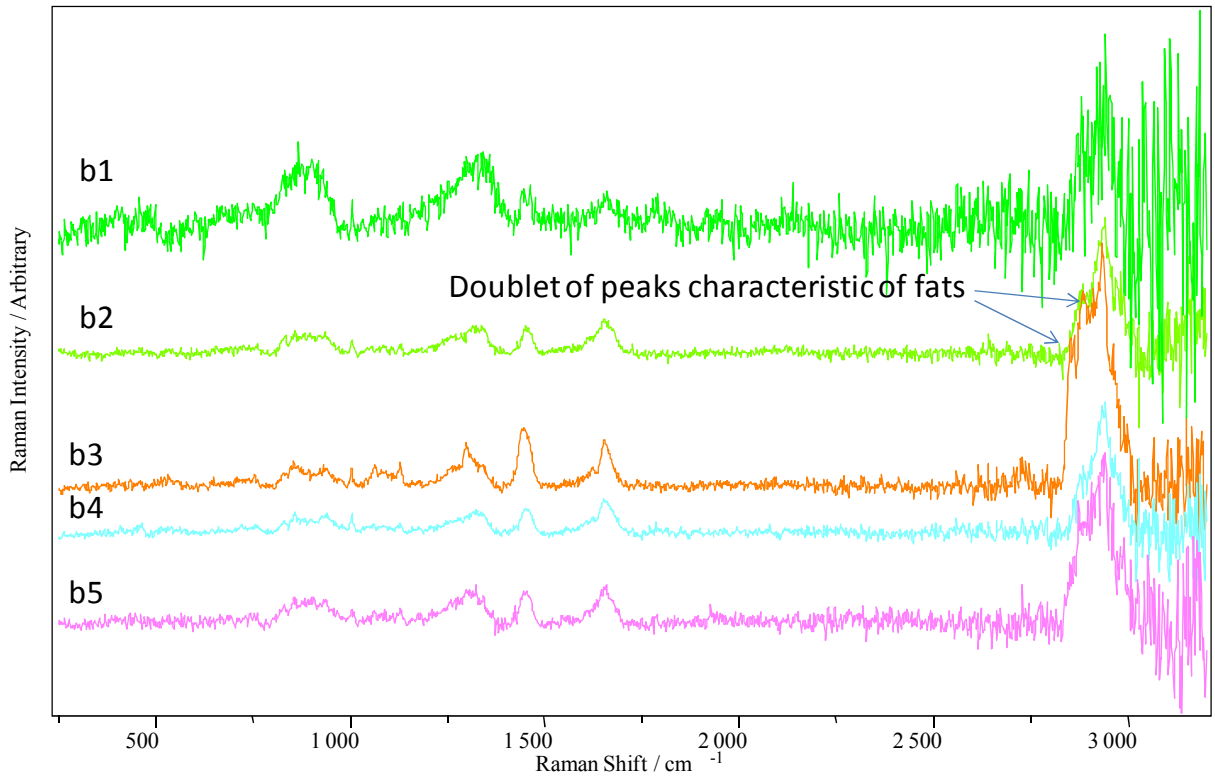

b1: spectrum with considerable noise; b2 & b4: spectra typical of protein (lean); b3: spectrum with peaks characteristic of adipose tissue; b5: spectra with peaks characteristic of protein and fat

Table 7 shows the correlation coefficients for the prediction of WBSF and consumer scores using Raman spectroscopy. The correlation coefficients were low and generally unsuitable for practical prediction of WBSF and consumer assessment of beef. The only statistically significant model was the prediction of juiciness. The model for juiciness when compared to actual values (Figure 17) only explained 8.5% ($R^2 = 0.085$) of the variation in the juiciness scores.

Table 7 – Prediction models developed for WBSF and consumer scores using Raman spectroscopy

Parameter	n	Signif	R^2 validation[a]	RMSEP	RMSEP as % mean
WBSF D14	112	ns	NA	NA	NA
Tenderness D14	144	ns	NA	NA	NA
Juiciness	110	**	0.104	11.08	22.7
Flavour	111	ns	NA	NA	NA
Overall liking	112	ns	NA	NA	NA

*Signif: statistical significance, ns: not statistically significant, * p<0.05, ** p<0.01, ***p<0.001: n number of observations used to validate model; NA Validation not applicable as calibration not statistically significant*

Figure 17 – Relationship between predicted juiciness and juiciness assessed by consumers

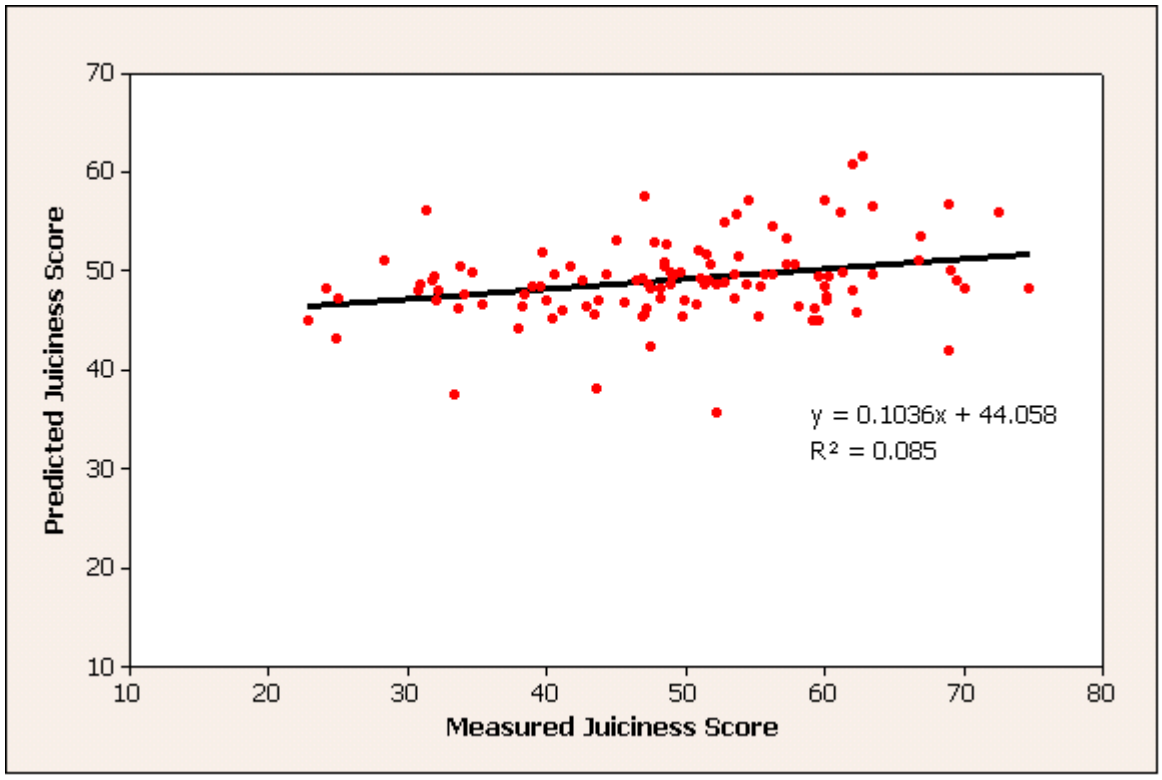

The prediction models for parameters related to fat content and fatty acid profile (Table 8) were much better than for meat quality (Table 7). Table 8 shows the statistically significant models obtained for the prediction of all fatty acid parameters evaluated except for PUFA. In general the Raman response to molecular vibrations associated with fat is much greater than for protein; thus, relatively small increases in intramuscular fat content can significantly increase the Raman signal for the spectral aspect related to fat (curve b3 in Figure 16). The regression coefficients used to develop the model for marbling show evidence that the Raman wavelength shifts (cm^{-1}) used in the prediction model are associated with fat rather than protein bands (Figure 18). The average standard error of prediction (RMSEP) for marbling score (60 units) represents an error of 17.6% when expressed as percentage of the mean marbling score (Table 8). Since marbling scores are subjective, a difference of 50 between trained assessors is considered, and the limit of difference between trained assessors for marbling, this error is of similar magnitude. Figure 19 shows the relationship between actual marbling scores and predicted marbling scores, which accounted for 41% of the variation in marbling score ($R^2 = 0.41$).

Although statistically significant models were obtained to predict %IMF, MUFA, SFA and CLA, the R^2 values for the validation were low and explained 19 to 26% of the variation in the measured values (see Figure 28 to Figure 31 in Appendix 3).

Table 8 – Prediction models developed for fat parameters using Raman spectroscopy

Parameter	n	Signif	R^2 validation	RMSEP	RMSEP as % mean
Marbling	110	***	0.427	61.02	17.6
% IMF	108	***	0.234	1.37	46.1
MUFA	109	***	0.273	5.53	48.3
PUFA	110	ns	NA	NA	NA
SFA	110	***	0.235	6.08	46.7
CLA	109	***	0.206	0.12	35.8
Trans	110	ns	NA	NA	NA

*Signif- statistical significance, ns not statistically significant, * p<0.05, ** p<0.01, ***p<0.001: n number of observations used to validate model; IMF intramuscular fat*

Figure 18 – Regression coefficients used for prediction of marbling score

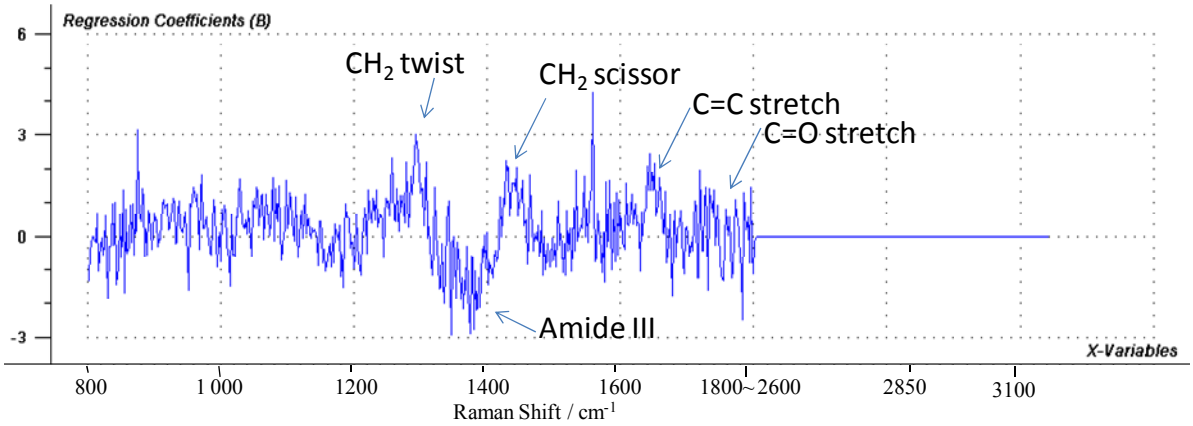

Regression coefficients used to predict marbling. Does use fat vs protein bands

Figure 19 – Relationship between actual marbling scores and those predicted by Raman Spectroscopy

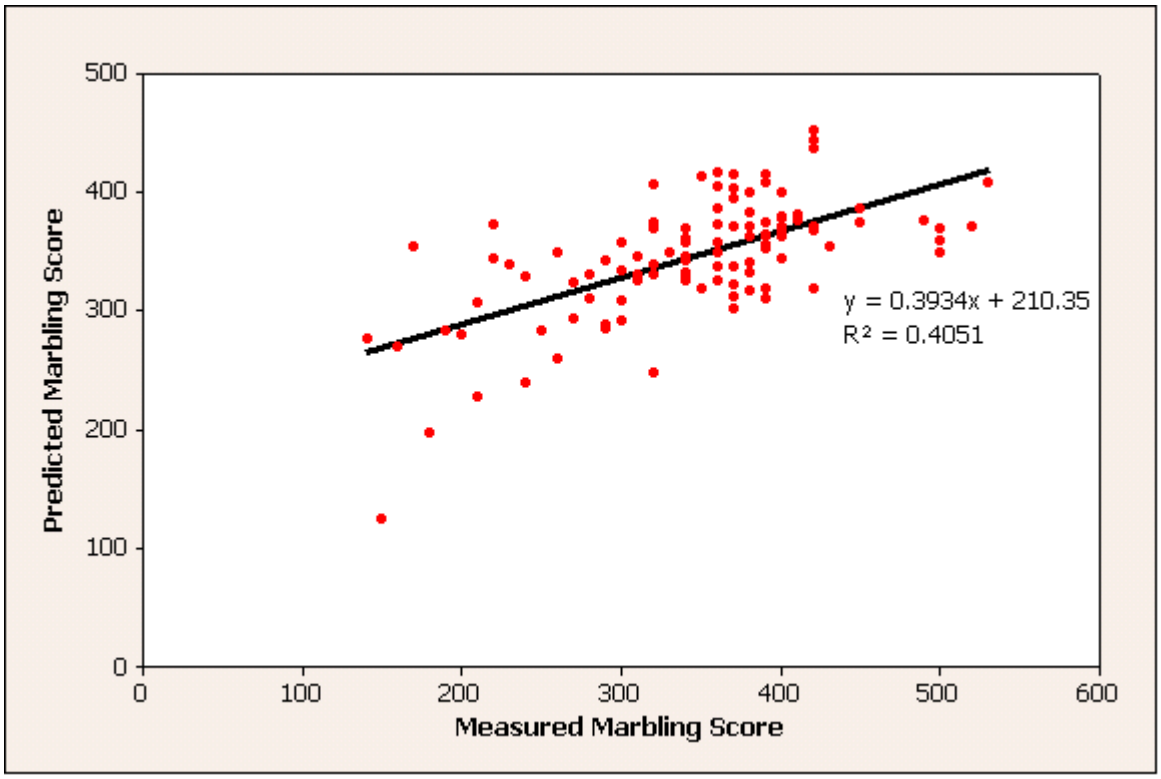

The regression coefficients used in the model for %IMF (Figure 20), MUFA (Figure 21) and SFA (Figure 22) show similarities in the wavelength shifts selected for the model. The position of the wavelengths with higher correlation coefficients corresponds to spectral peaks associated with lipid characteristics, namely the ester linkage (1750 cm^{-1}), unsaturated bonds (1660 cm^{-1}) and aliphatic deformation modes (1300 and 1440 cm^{-1}). The regression coefficients associated with protein (amide 3) are negative, which would be expected since, as intramuscular fat increases, protein would decrease.

Figure 20 – Regression coefficients used for % intramuscular fat prediction

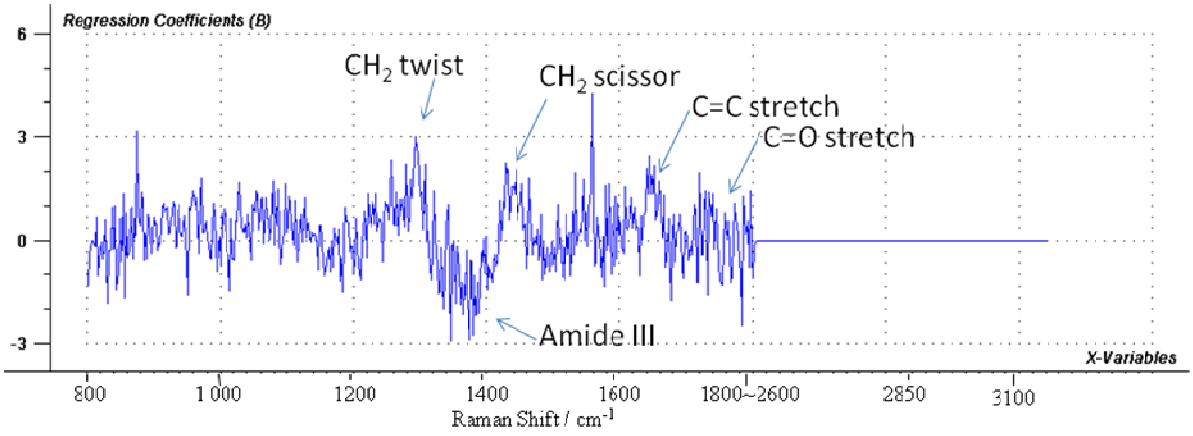

Figure 21 – Regression coefficients used for prediction of MUFA

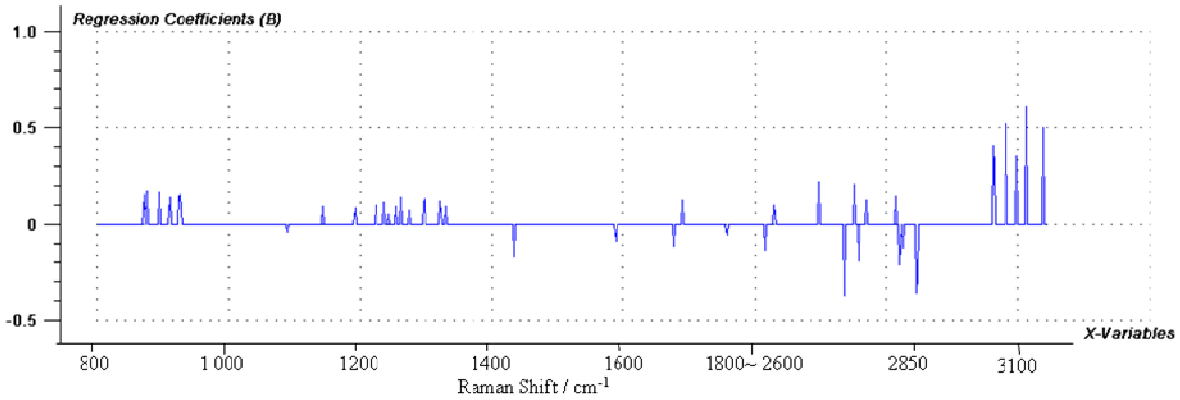

Figure 22 – Regression coefficients used for prediction of SFA

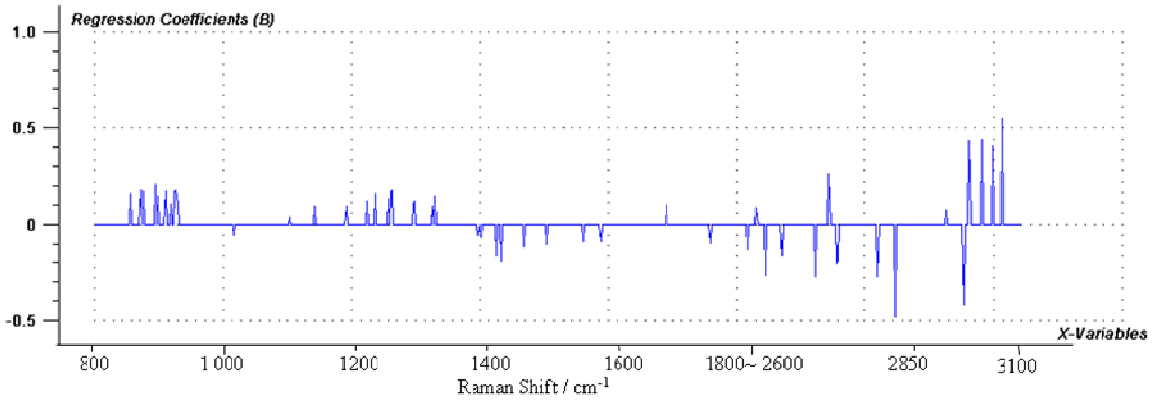

Raman spectra of adipose tissue result in good models for the prediction of individual fatty acid profiles (Beattie *et al.* 2006b). Predictions of groups of similar fatty acids (SFA, MUFA, etc.) were not expected due to the relatively low content of fat in beef LD. In the present study it is considered that the Raman spectra obtained are influenced by the amount of marbling in the samples and the predictions of SFA and MUFA obtained are because these are related to the marbling content and IMF content of the samples. In this study all the individual spectra obtained for each sample (a matrix of 49 individual spot collections) was co-added during the spectral acquisition to give one representative spectrum. Given the small sampling spot of the Raman spectrometer it is possible to obtain spectra of marbling fat or lean separately. In the current study acquiring each position in the sample matrix as individual spectra would have resulted in around 7,000 spectra to be individually evaluated, compared to 150 when co-added. This would considerably increase the time required for data manipulation of the spectra (e.g. background correction, preparation for statistical modelling etc.), but if marbling spectra could be obtained independently then such spectra could be used to predict fatty acid profiles.

4.5 Relationship between Warner-Bratzler shear force and consumer acceptability.

The results of the logistic regression for day 14 based on the acceptability of individual consumer responses are given in Figure 23. Table 9 gives the statistical parameters for the model. The important parameters are the percent correctly classified by the model (PC%) and the C-statistic. If the C-statistic is less than 0.5 then there is no discrimination between the two satisfaction categories; values of C between 0.7 and 0.8 are considered to indicate a fit which is acceptable for use in classification and C>0.8 indicates an excellent classification model. The model fitted for individual scores was good, correctly classifying 72% of the observations with a relatively high C-statistic (0.684). Figure 23 shows that there is a 70% probability that consumers would consider steaks with WBSF values of around 5.5 kg force acceptable. The upper and lower limits of this prediction are 67% and 74%.

The logistic regression based on classifying a sample as acceptable when more than 2/3 of the consumers found a particular sample acceptable is shown in Figure 24 The model fitted on the basis of 2/3 responses correctly classified 82% of the responses and had a high C-statistic (0.8 in Table 9), indicating an excellent classification model.

Figure 23 – Relationship between probability of acceptance of steaks and Warner-Bratzler shear force calculated using logistic regression based on individual responses

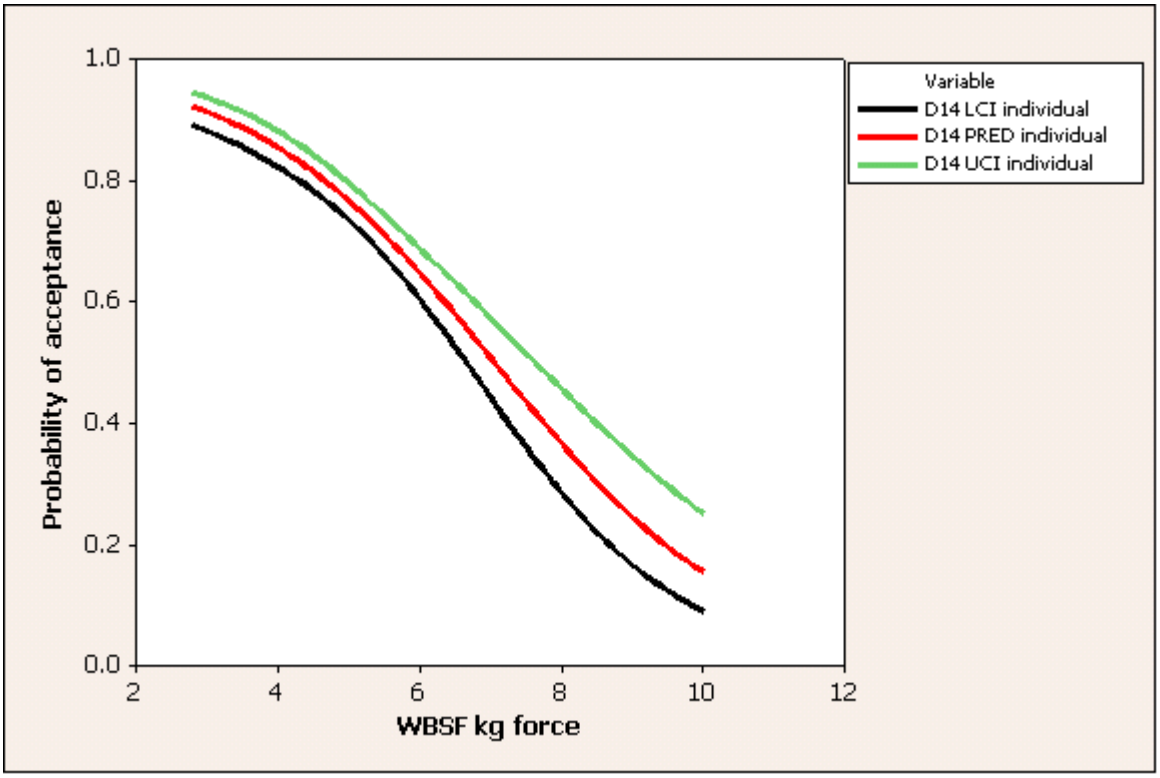

PRED: predicted line, LCI: lower confidence limit, UCI: upper confidence limit

Figure 24 – Relation between probability of acceptance of steaks and Warner-Bratzler shear force calculated using logistic regression based on 2/3 decision (Platter *et al., 2003*)

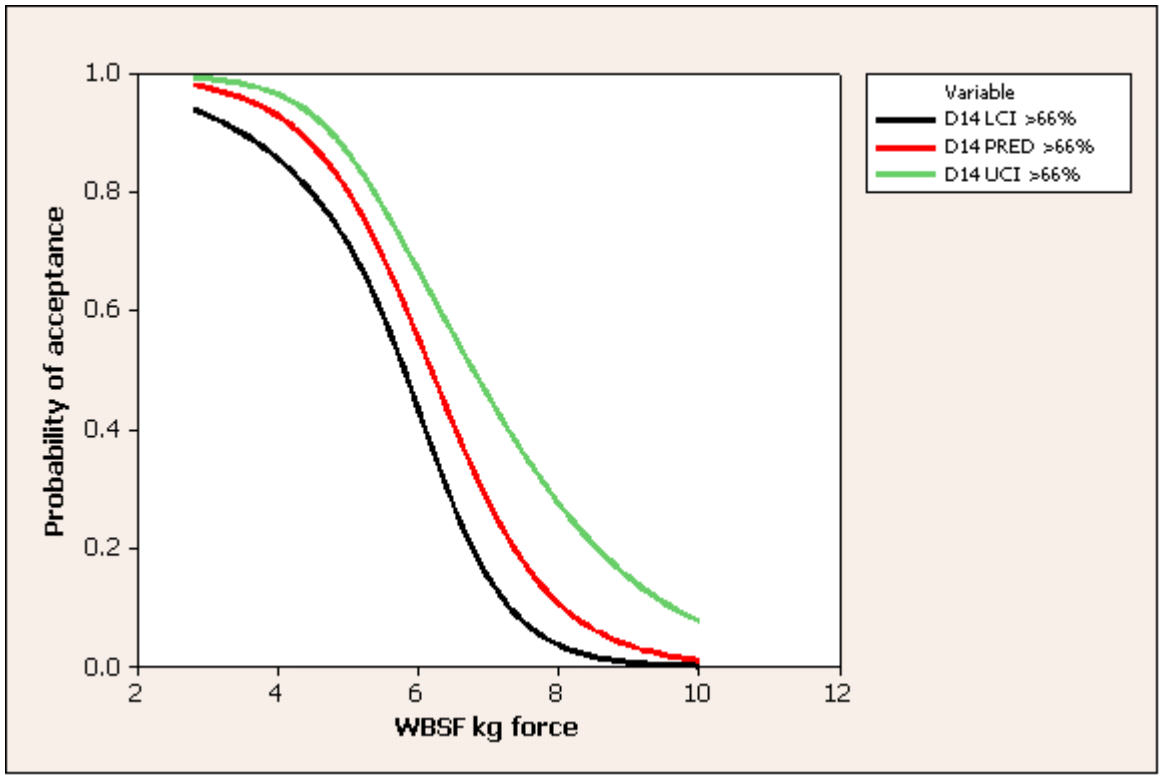

Table 9 - Statistical parameters indicating validation of fitted model for classifying acceptability of steaks aged for 14 days

Model	Day	Significance	R^2	PC%	C-statistic
Individual panellist	14	***	0.095	72.61	0.684
>66% response	14	***	0.296	81.25	0.805
Platter *et al.*	14	NA	0.225[a]	66.70	0.738

[a] *Different methods were used by Platter et al. (2003) to calculate R^2 compared to the current study and therefore the R^2 values cannot be directly compared.*

Figure 25 compares the two models (individual responses and greater than 2/3) with the model reported by Platter *et al.* (2003). The individual and 2/3 models intersect at around 70% acceptability with shear force values of approximately 5.4 kg force. Above a value of 5.4 kg force (the crossover point of the two current models) the model based on individual responses predicts greater acceptability than the model based on >2/3 decision model (Figure 25). For example, using the individual response model a WBSF value of 4 kg force is predicted to be 95% acceptable, whereas on the > 2/3 decision model the acceptability is predicted to be 86% (Figure 25). Below 4 kg force the acceptability predicted by the individual model is lower than the acceptability predicted by the >2/3 decision model.

Figure 25 – Comparison of logistic regression models from current study with that of Platter *et al.* (2003)

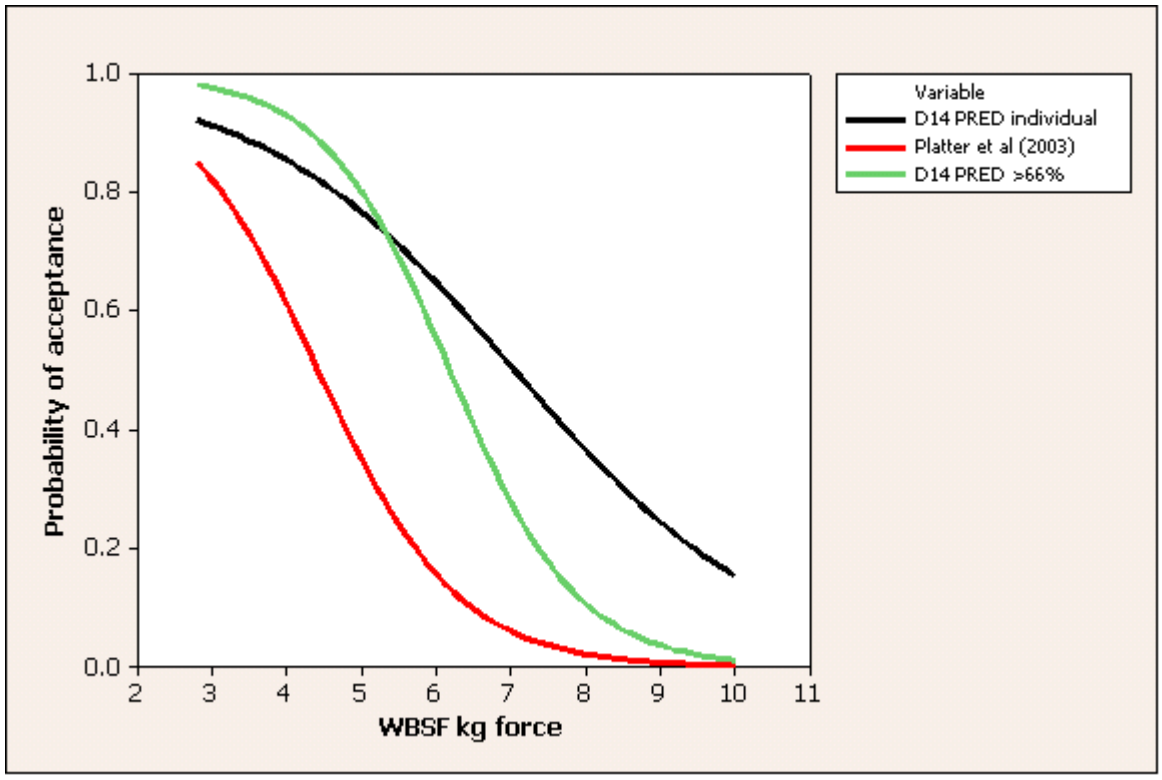

In all cases the model developed by Platter *et al.* (2003) in the US resulted in lower acceptability ratings for any given WBSF value than the models currently developed. Thus steaks of around 5.4 kg force rated as 70% acceptable by Northern Ireland consumers would only be rated as 30% acceptable according to the US model. This large difference between the models could represent a difference of methodological approaches and differences in consumer acceptability between the two countries. A summary of the differences between the methodologies of Platter *et al.* (2003) and the current approach are given in Table 10.

In the current study WBSF values were measured on samples which had been stored at 2^{o}C for 14 days, whereas Platter *et al.* (2003), although they aged their samples under similar conditions, froze them and subsequently thawed them prior to determination of WBSF (Table 10). For determination of WBSF values Platter *et al.* (2003) essentially cooked their samples rapidly (6 min) to a target endpoint temperature (EPT) of 70^{o}C, compared to the present study which used a relatively slow cook to achieve an internal temperature of 70^{o}C.

Lagerstedt *et al.* (2006), using a similar water bath cooking method for WBSF as in the current studies, observed lower WBSF values in steaks previously frozen than in fresh steaks. The decrease due to prior freezing was around 0.7 kg force, with previously frozen values around 13% lower than fresh values. Shanks *et al.* (2002), using an open hearth broiler to cook steaks for WBSF, observed similar decreases in WBSF due to prior freezing. Van Oeckel *et al.* (1999) found that pork samples aged for 48 hours and cooked using a water bath procedure had lower WBSF values (28.6 N, 2.9 kg force) than steaks previously frozen and cooked using a grilling method to internal temperature of 74^{o}C (35.3 N, 3.9 kg force). It is therefore difficult to establish whether differences in WBSF methodology can account for the

differences between the Platter model and current model since the reports of Lagerstedt *et al.* (2006) and Shanks *et al.* (2002) could account for the Platter model being shifted to lower WBSF values, but only by about 0.7 kg force. The data of Van Oeckel *et al.* (1999) would however indicate a shift to higher WBSF in frozen grilled steaks used by Platter *et al.* (2003) compared to water bath cooked fresh steaks (method used in current study).

The main difference in consumer evaluation is the method of cooking, where Platter *et al.* (2003) used a longer cook time to achieve an endpoint temperature of 70^{o}C cooking compared to a quicker cook to achieve a higher endpoint temperature of 80^{o}C in the current study. The steaks cooked in the current study visually appeared as well done; however when steaks cooked to medium were assessed by consumers who preferred their steaks as medium, or steaks cooked well done by consumers preferring this way, there was little difference in consumer scores (Farmer *et al.* 2009a). Cox *et al.* (1997) also noted that higher scores were given when consumers were presented with steaks which matched their preferred degree of doneness.

Table 10 - Comparison of methodology of Platter *et al.* (2003) and current study

Platter comparison	Platter *et al.*	AFBI
	WBSF	
Aging	14 days	14 days
Physical state	Frozen-thawed	Fresh (not frozen)
Cooking Method	Conveyor grill, 6 min at 176°C, endpoint 70°C	Water bath at 75°C, for 50 minutes, endpoint 70°C, cooled in ice stored at 2°C
	Consumer test	
Meat	2.54 cm thick slice, thawed at 2°C for 24 hour	2.54 cm thick slice, thawed at 2°C for 24 hour
Cooking	Grilled 15 minutes, both sides, endpoint temperature 70°C	Clam shell grill, 7 minutes, both sides, endpoint temperature 80°C
Serving	Kept at 49°C prior to serving, time not specified	Served within 1 minute of cooking

Farmer *et al.* (2009a) found that when Australian and Northern Ireland consumers were compared using the same cooking and consumer protocols, Northern Ireland consumers gave slightly higher scores for juiciness and overall satisfaction than Australian consumers. Farmer *et al.* (2009b) noted that Northern Ireland consumers rated flavour at least as important as tenderness if not more so in relation to overall liking of beef. Hence, it is difficult to identify any one factor to account for the differences between the model derived by Platter *et al.* (2003) and the model developed in the current study.

5 Conclusions

1. Hyperspectral imaging can result in image acquisition from a forerib in a short time and as such would be suitable for on-line application if suitable robotic systems could be developed to move the cut quartered surface past the imaging camera.

2. Hyperspectral imaging gave prediction models based on a much larger area (all of the LD) than previous NIR systems and the prediction models developed were generally better than other published data for non-imaging systems.

3. Hyperspectral imaging was able to discriminate lean and fat regions, enabling separate spectra to be measured for each.

4. Prediction of fatty acid profiles by using hyperspectral imaging from the identified marbling fat gave good prediction models for some aspects of the fatty acid profiles. Further work is required to develop models for individual fatty acids in the profile.

5. Raman spectroscopy from spectra acquired at 2 days resulted in poor predictions of meat quality but acceptable predictions of fatty acid profiles. Further work is required to develop optimal systems for acquisition of Raman spectra before this could be applied on-line.

6. Good statistical models were developed showing the relationship between Warner-Bratzler shear force and consumer evaluation. Further work is required to understand the difference between the models developed in this project and those for US consumers.

6 Acknowledgements

This joint AFBI, Campden BRI project was initiated from discussions between Prof. Samuel Millar, Bruce Moss and Kim Matthews. The authors thank EBLEX for their support of the project.

This work could not have been undertaken without the excellent contribution of the Beef Eating Quality team at AFBI; Mr Ernie Tolland for organising the sampling at the meat plant and planning of the consumer trials and validating data; Joan Tollerton for undertaking the consumer trials and consumer data collection and validation; Mr Declan Devlin for carcass and meat quality measurements and Hollie Embleton for support in sample preparation and shear force measurements.

Thanks are also due to Mr. Tony McBride for determining the sampling matrix for the Raman measurements and undertaking the measurements and Alan Beattie and Sharon Stewart for undertaking the fatty acid analysis. A number of other staff also assisted in the consumer trials and their help is acknowledged.

Thanks are due to Jonathan Birnie, Dunbia Meats, for agreeing to collaborate in this project. The cooperation and help of a number of staff at Dunbia Meats during the project is acknowledged.

7 References

Alfaia, C. P. M., Alves, S. P., Martins, S. I. V., Costs, A. S. H., Fontes, C. M. G. A., Lemos, J. P. C., Bessa, R. J. B. and Prates, J. A. M. (2009). Effect of feeding system on intramuscular fatty acids and conjugated linoleic acid isomers of beef cattle, with emphasis on their nutritional value and discriminatory ability. *Food Chemistry* **114:**939-946.

Barnes, R. J., Dhanoa, M. S. and Lister, S. J. (1993). Correction to the description of standard normal variate (SNV) and de-trend (DT) transformations in *Practical Spectroscopy with Applications in Food and Beverage Analysis*, 2nd Edition. *Journal of Near Infrared Spectroscopy* **1:**185-186.

Beattie, J. R., Bell, S. E. J. and Moss, B. W. (2004a). A critical evaluation of Raman spectroscopy for the analysis of lipids: fatty acid methyl esters. *Lipids*, **39:**407-419.

Beattie, J. R., Bell, S. J., Farmer, L. J., Moss, B. W. and Patterson, D. C. (2004b). Preliminary investigation of the application of Raman spectroscopy to the prediction of sensory quality of beef silverside. *Meat Science*, **66(4):**903-913.

Beattie, J. R., Bell, S. E. J. and Moss, B. W. (2004c). Preliminary Raman spectroscopic investigation of the changes in beef sternomandibularis muscle during the thawing of muscle strips frozen pre-rigor. *50th International conference on Meat Science and Technology*, Helsinki, August. (Abstract)

Beattie, J. R., Bell, S. E. J., Borgaard, C., Fearon, A. M., Beattie, J. A. M. and Moss, B. W. (2006a). Discrimination of adipose tissue from different species using Raman Spectroscopy. *BSAS Annual Conference*, York, March, pp 24.

Beattie, J. R., Bell, S. E. J., Borgaard, C., Fearon, A. M. and Moss, B. W. (2006b). Prediction of adipose tissue using Raman spectroscopy: average properties and individual fatty acids. *Lipids*, **41(3):**287-294.

Beattie, J. R., Bell, S. E. J., Borggaard, C., Fearon, A. M. and Moss, B. W. (2007). Classification of adipose tissue species using Raman spectroscopy. *Lipids*, **42(7):**679-685.

Beattie, J. R., Bell, S. E. J., Borggaard, C. and Moss, B. W. (2008). Preliminary investigations on the effects of ageing and cooking on the Raman spectra of porcine longissimus dorsi. *Meat Science*, **80:**1205-1211.

Bligh, E. G. and Dyer, W. J. (1959). A rapid method of total lipid extraction and purification. *Canadian Journal of Biochemistry and Physiology*, **37(8):**911-917.

BSI (2001). *Animal and vegetable fats and oils*. Preparation of esters of fatty acids. Section 5 Trans-esterification method, BSI London, pp 7-9, **BS 684-2.34:2001**.

Cox, R.J., Thompson J.M., Cunial, C.M., Winter, S. and Gordon, A.J. (1997). The effect of degree of doneness of beef steaks on consumer acceptability of meals in restaurants. *Meat Science*, **45(1):**75-85.

Farmer, L. J., Devlin, D. J., Gault, N. F. S., Gee, A., Gordon, A. W., Moss, B. W., Polkinghorne, R., Thompson, J., Tolland, E. L. C. and Tollerton, I. J. (2009a). Effect of type and extent of cooking on the eating quality of Northern Ireland beef. *55th International Congress of Meat Science and Technology*, Copenhagen, August, PE7.33. (Abstract)

Farmer, L. J., Devlin, D. J., Gault, N. F. S., Gee, A., Gordon, A. W., Moss, B. W., Polkinghorne, R., Thompson, J., Tolland, E. L. C. and Tollerton, I. J. (2009b). Prediction of eating quality using the Meat Standards Australia system for Northern Ireland beef. *55th International Congress of Meat Science and Technology*, Copenhagen, August, PE7.34. (Abstract)

González-Martín, I., González-Pérez, N. Alvarez-García and J. M. González-Cabrera. (2005). On-line determination of fatty acid composition in intramuscular fat of Iberian pork loin by NIRS with a remote reflectance fibre optic probe. *Meat Science* **69:**243–248.

Lagerstedt, A., Marcazzani, M., Enfalt, L., Johansson, L., and Lundstrom, K. (2006). Does freezing positively or negatively affect shear force and sensory quality of beef. *Proceedings of the International Congress of Meat Science & Technology*, Dublin, pp 545-546.

Millar, S. J. and Hall, A. G. (2004). Assessment of chocolate blends using near infrared (NIR) spectroscopy. *Campden BRI R&D Report* No. 205.

Millar, S. J., Whitworth, M. B. and Chau, A. (2008). Mapping food composition using NIR hyperspectral imaging. *New Food* **11(3):**34-39.

Moss, B.W., Gordoen, A., Matthews, K., Homer, D. and Hadley, P. (2009). Potential of NIR spectroscopy for prediction of tenderness of beef sirloin. *Proceedings of the British Society of Animal Science*. Southport, pp 114.

Naganathan, G. K., Grimes, L. M., Subbiah, J., Calkins C.R., Samal, A. and Meyer, G. E. (2008). Visible/near-infrared hyperspectral imaging for beef tenderness prediction. *Computers and Electronics in Agriculture* **64(2):**225-233.

Osborne, B. G., Fearn, T. and Hindle, P. H. (1993). Practical NIR spectroscopy with applications in food and beverage analysis, 2nd Edition, Longman Scientific & Technical, Harlow, England.

Platter, W. J., Tatum, J. D., Belk, K. E., Chapman, P. L., Scanga, J. A., and Smith G. C. (2003). Relationships of consumer ratings, marbling score, and shear force value to consumer acceptance of beef striploin. *Journal of Animal Science* **81:**2741-2750.

Paul, A. A. and Southgate, D. A. T. (1976). McCance and Widdowson's The Composition of Foods, 6th edition, Her Majesty's Stationery Office.

Prieto, N., Roehe, R., Lavin, P. Batten,. G. and Andrese, S. (2009). Application of near infrared spectroscopy to predict meat and meat products quality: A review. *Meat Science*, **83**:175-186.

Realini, C. E. Duckett and S. K. Windham W. R. (2004). Effect of vitamin C addition to ground beef from grass-fed or grain-fed sources on color and lipid stability, and prediction of fatty acid composition by near-infrared reflectance analysis. *Meat Science* **68**:35-43.

Shackelford, S. D., Wheeler, T. L., and Koohmarie M. (2004). Development of optimum protocol for visible and near-infrared reflectance spectroscopic evaluation of meat quality. *Meat Science* **68**:371-381.

Shackelford, S. D., Wheeler, T. L., and Koohmarie M. (2005). On-line classification of US select beef carcasses for longissimus tenderness using visible and near infrared reflectance spectroscopy. *Meat Science* **69**:409-415.

Shanks, B. C., Wulf D. M. and Maddock R. J. (2002). Technical note: The effect of freezing on Warner-Bratzler shear force values of beef longissimus steaks across several postmortem aging periods. *Journal of Animal Science* **80:**2122-2125.

Sierra, V., Aldai N., Castro, P., Osoro, K., Coto-Montes, A. and Oliván M. (2008). Prediction of the fatty acid composition of beef by near infrared transmittance spectroscopy. *Meat Science* **78:**248-255.

Van Oeckel, M. J., Warnants, N. and Boucqué, Ch. V. (1999). Pork tenderness estimation by taste panel, Warner–Bratzler shear force and on-line methods. *Meat Science* **53(4):**259-267.

Warren, H. E., Scollan, N. D., Enser, M., Hughes, S. I., Richardson, R. I. and Wood, J. D. (2008). Effects of breed and a concentrate or grass silage diet on beef quality in cattle of 3 ages. I: Animal performance, carcass quality and muscle fatty acid composition. *Meat science* **78**:256-269.

8 Appendix 1 Carcass & meat quality: sex type differences

Figure 26(a) to (f) shows the distribution of Warner-Bratzler shear force values for the three sex types initially sampled. Table 11 gives a summary of carcass quality and meat quality parameters for those carcasses with pHu less than 5.8 (i.e. those used for the prediction model). Bulls had the highest hot carcass weight (HSCW) and heifers the lowest hot carcass weight (see Table 12). Bulls had significantly lower marbling score, higher pHu, and higher WBSF values than heifers or steers (see Table 12). The statistical analysis in Table 12 does not include carcasses with pHu > 5.8, and the difference in mean pHu of the bulls to other sex types is small. Further evaluation of the relationship between pHu is required as in the Meat Standards Australia (MSA) system for which carcasses with pHu > 5.72 are excluded.

Figure 26 - Distribution of Warner-Bratzler shear force values

(a) Warner-Bratzler shear force values for bulls – 14 day

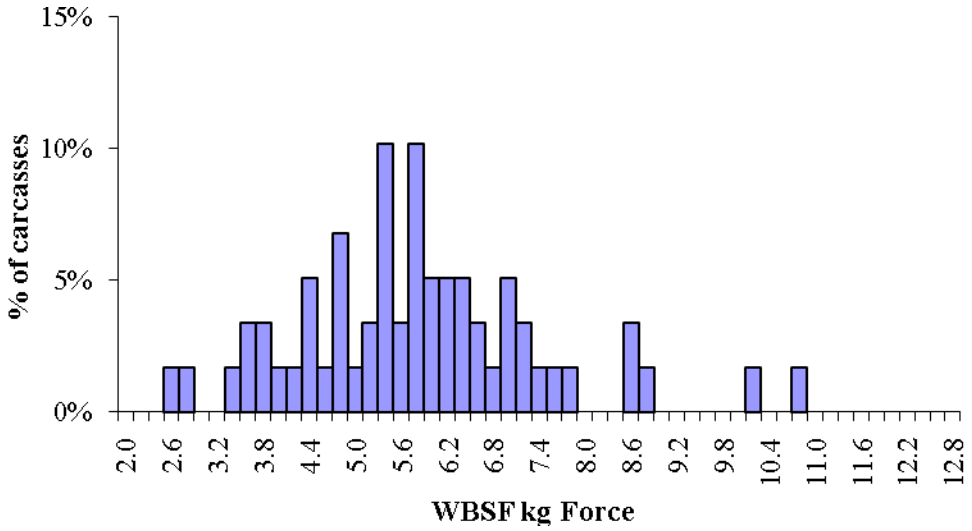

(b) Warner-Bratzler shear force values for bulls – 21 day

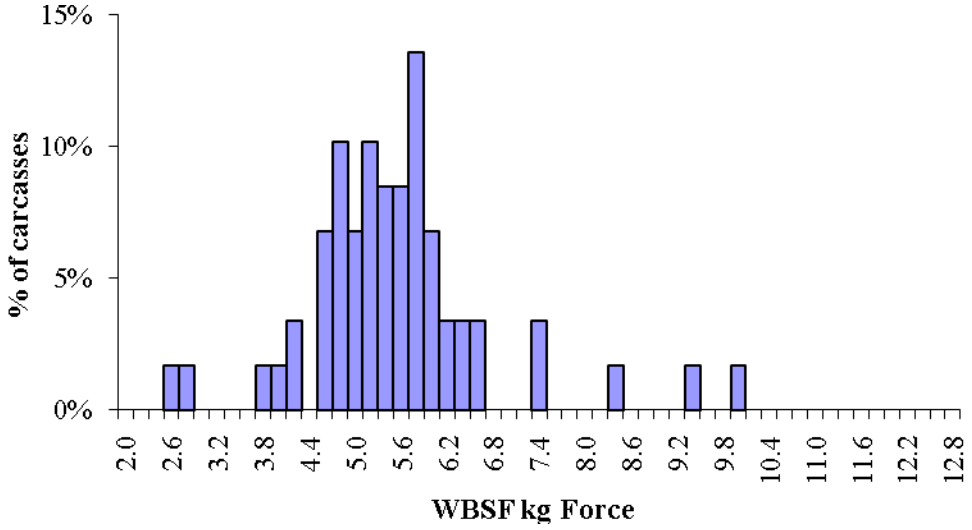

(c) Warner-Bratzler shear force values for steers – 14 day

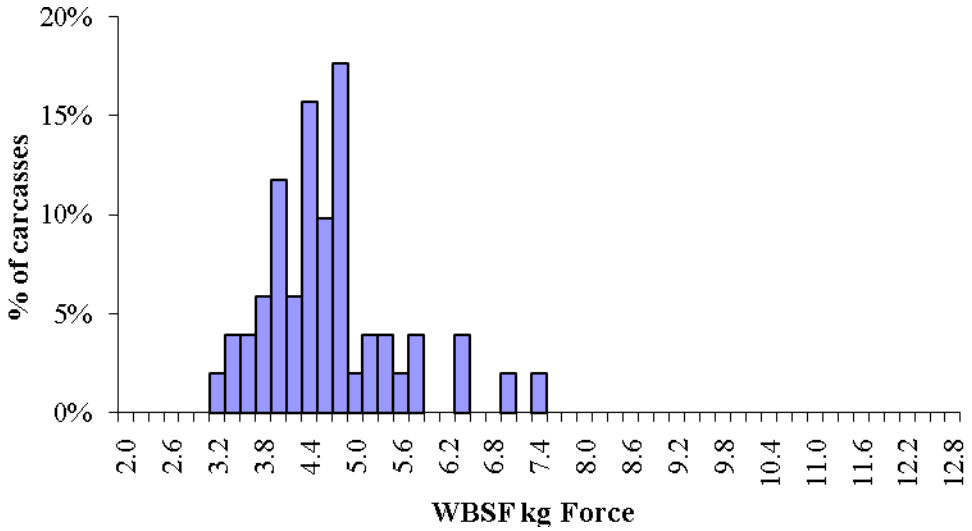

(d) Warner-Bratzler shear force values for steers – 21 day

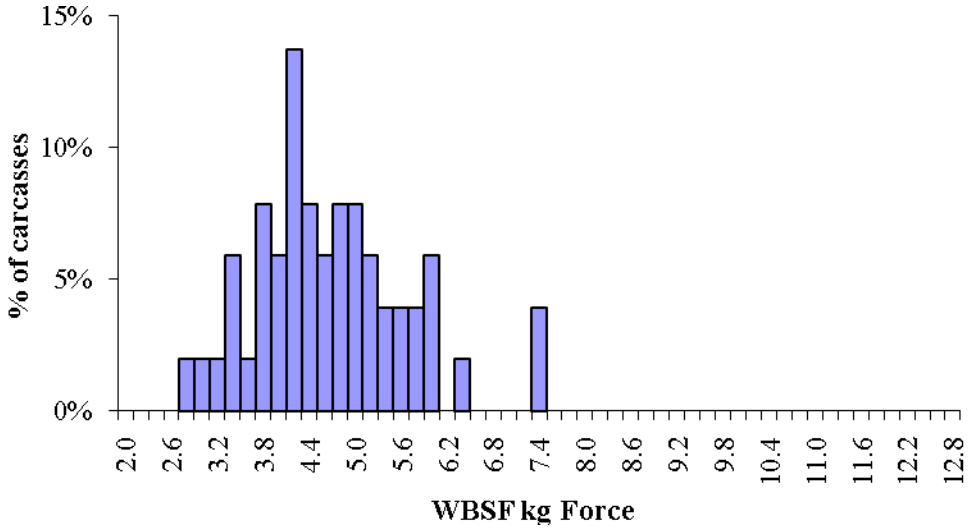

(e) Warner-Bratzler shear force values for heifers – 14 day

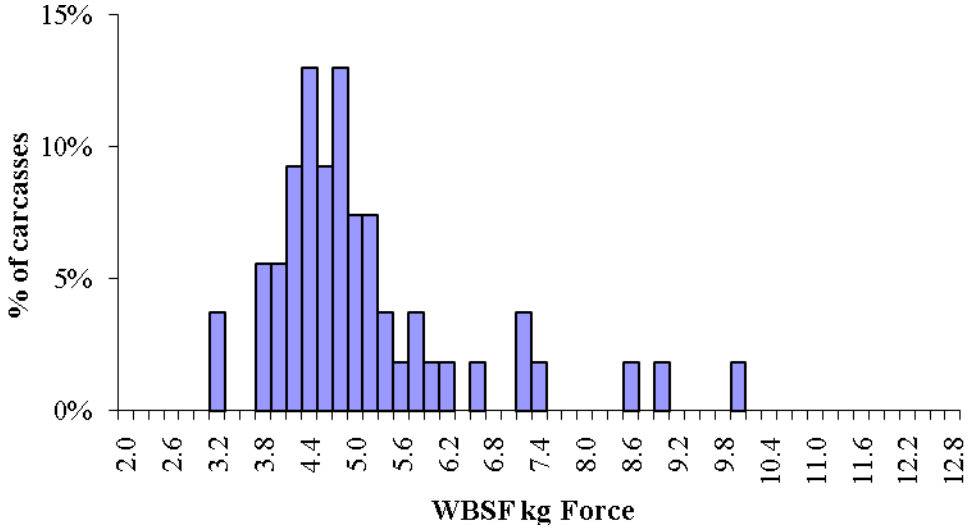

(f) Warner-Bratzler shear force values for heifers – 21 day

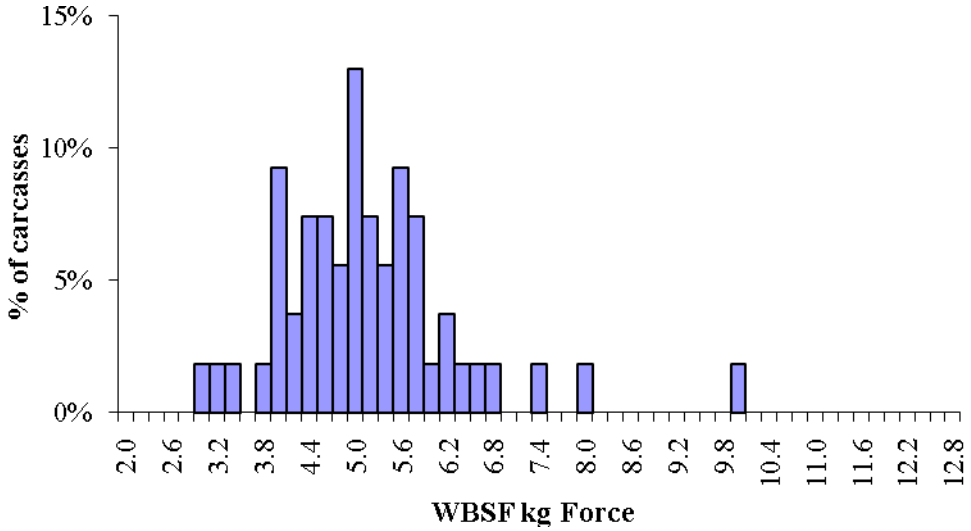

Table 11 - Summary of meat quality parameters for Bulls, Heifers & Steers

Parameter	n	Mean	SD	Min.	Max.
Bulls					
HSCW (kg)	47	411.5	48.1	319.8	530.6
MSA Marbling score	48	299.2	86.3	140.0	480.0
pH Probe	48	5.6	0.1	5.5	5.8
% Cooking loss D7	48	29.3	2.7	21.6	34.3
WBSF D7 mean (kg)	48	6.0	1.1	3.8	8.5
% Cooking loss D14	48	27.3	4.8	21.6	54.6
WBSF D14 mean (kg)	48	6.0	1.3	3.4	10.1
Heifers					
HSCW (kg)	52	324.9	35.8	247.4	439.6
MSA Marbling score	52	369.0	53.3	260.0	500.0
pH Probe	52	5.6	0.0	5.5	5.7
% Cooking loss D7	52	27.5	2.4	22.6	32.9
WBSF D7 mean (kg)	52	5.4	1.3	2.9	10.8
% Cooking loss D14	52	26.2	2.1	20.7	31.6
WBSF D14 mean (kg)	52	5.1	1.2	3.2	10.0
Steers					
HSCW (kg)	50	376.5	36.8	324.2	520.6
MSA Marbling score	50	368.6	67.2	210.0	540.0
pH Probe	50	5.6	0.0	5.5	5.7
% Cooking loss D7	50	28.2	2.0	24.7	32.0
WBSF D7 mean (kg)	50	4.9	1.0	3.2	7.9
% Cooking loss D14	50	26.1	2.0	20.2	29.8
WBSF D14 mean (kg)	50	4.7	0.9	3.1	7.5

Table 12 – Effect of sex type on meat quality parameters (note: this analysis excludes carcasses with pHu> 5.8)

Meat Quality	Bulls	Heifers	Steers	Significance
HSCW (kg)	411.5[a]	324.6[b]	376.5[c]	***
Marbling score	299.2[a]	368[b]	368.6[b]	***
pHu	5.59[a]	5.57[b]	5.57[b]	*
% Cooking loss D14	27.3	26.2	26.1	ns
WBSF D14 (kg)	5.97[a]	5.05[b]	4.66[b]	***

Means with common superscripts are not significantly different (p<0.05)
*ns not statistically significant ,p>0.05; * p<0.05;** P,0.01; ***p<0.001.*

9 Appendix 2 Further evaluation of Raman spectra

The Raman spectra used for prediction were the accumulation of a matrix of 49 individual points (see method). The Raman was focused on the first point acquired and this focal distance was used for all other points in the matrix of spectra to be collected and co-added to produce the final spectrum. Care was taken to keep the cut surface of the meat flat so that this focus would apply to spectra acquired at other points in the matrix. To use Raman autofocus at each point would increase the total acquisition time and it was considered appropriate, given the small spectral area measured at each point, to have as many points as feasible to produce a representative spectrum. Previous work on the current Raman spectrometer had indicated that this would yield good spectra for meat. Therefore, a balance was required to keep the overall acquisition down to a reasonable time in order to measure the desired number of samples on any one day.

Following the evaluation of the data and the high noise to signal ratio it was decided to see if different lens systems could reduce the noise relative to the signal. Between the completions of the Raman measurements in the project the Raman spectrometer underwent its annual service. The service engineer identified a cooling fan with an intermittent problem which could have resulted in increased spectral noise; all other calibrations and laser power were within specification. A number of spectra were acquired with different lens systems and also with the same lens as used during the project. During this evaluation 30 spectra were acquired at different spacing 4 mm apart with both manual focus (video camera) and Raman auto focus for each spectrum. This is different to the experimental procedure where focus was used on the first spectral collection but then all other spectra were acquired using the same focus. Figure 27 shows the average spectra of these recently acquired 30 spectra (data acquired to reduce noise post-service), the average of all spectra acquired during the project and spectra acquired on a different spectrometer used for the papers published by Beattie *et al.* The current spectra acquired post-service show considerably less noise than those acquired during the project and are of comparable quality to those of the Raman spectrometer where reliable predictions of meat quality have been obtained (Beattie *et al.* 2004b and 2008). The spectra acquired to test for noise reduction were for samples aged for 14 days rather than 2 days used in the project; however, it has previously been shown that good quality spectra could be obtained at even earlier times post mortem, e.g. 1 hour (Beattie *et al.* 2004c.). The improvement in quality and reduction of noise may have been related to a problem associated with the cooling fan prior to routine service or may be related to the Raman focus being more sensitive to variations in sample height from the first autofocus point. Raman spectrometry is more routinely used for examination and quality assurance of pharmaceutical products than biological materials such as meat. Discussions have been initiated with the equipment supplier to improve the quality of the spectra from meat samples.

Figure 27 – Comparison of spectra acquired during project with published spectra and recently acquired spectra

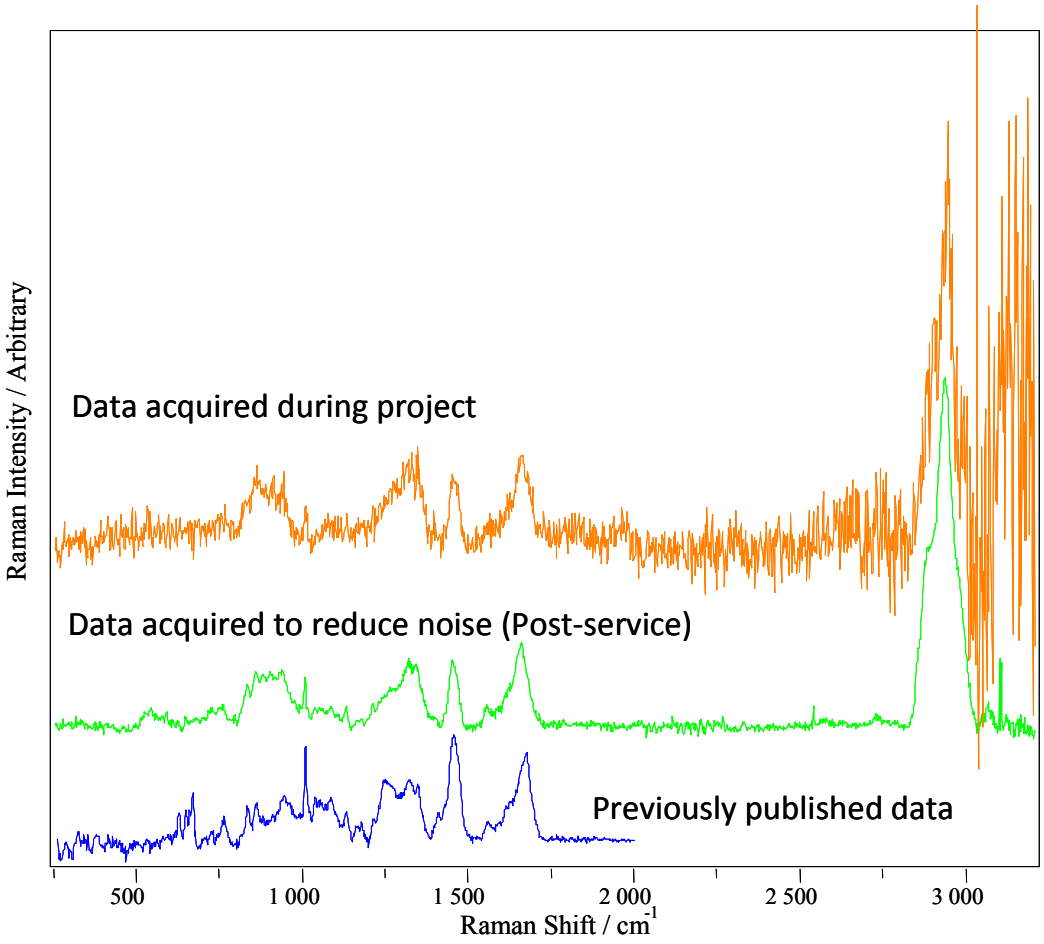

Further work is required to develop a measurement probe suitable for on–line prediction of meat quality using Raman spectrometry. It is anticipated that the improvement in signal quality after the repair would allow much more robust calibrations, comparable in quality to those previously published (Beattie *et al.* 2004b and 2008).

10 Appendix 3 Prediction models for IMF, MUFA, SFA and CLA

Figure 28 – Relationship between measured intramuscular fat content and intramuscular fat predicted by Raman Spectroscopy

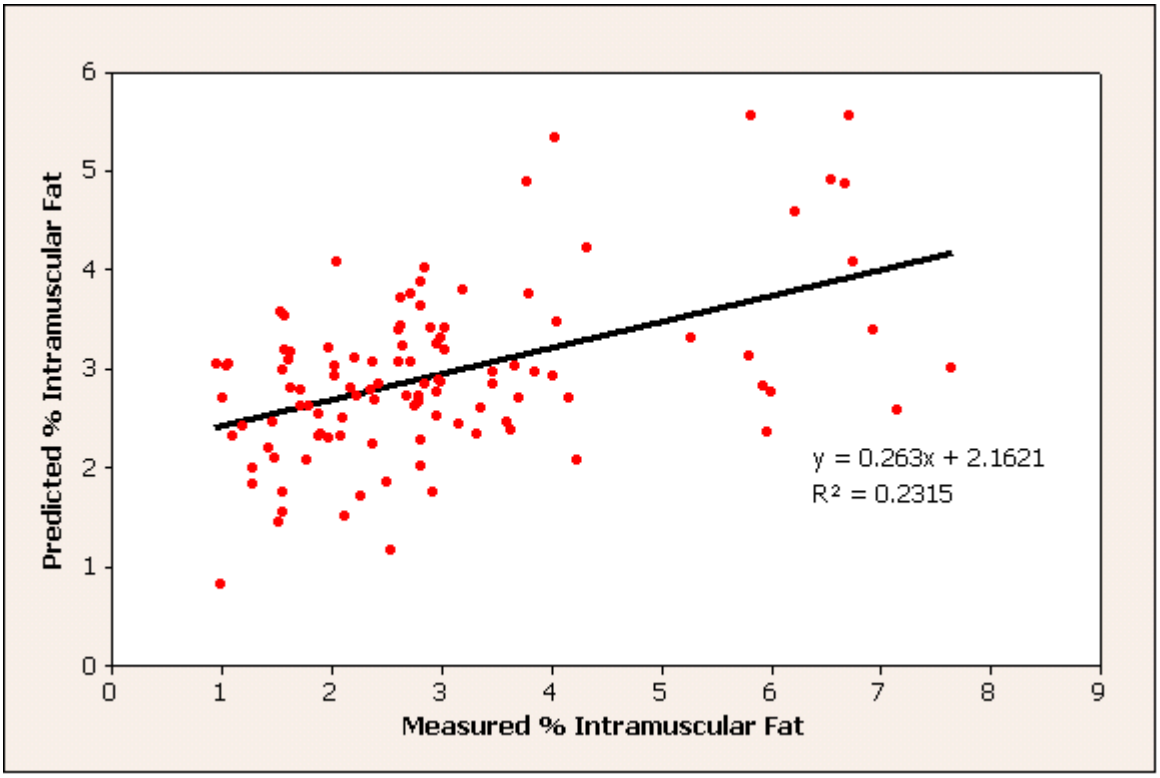

Figure 29 – Relationship between measured MUFA and MUFA predicted by Raman Spectroscopy

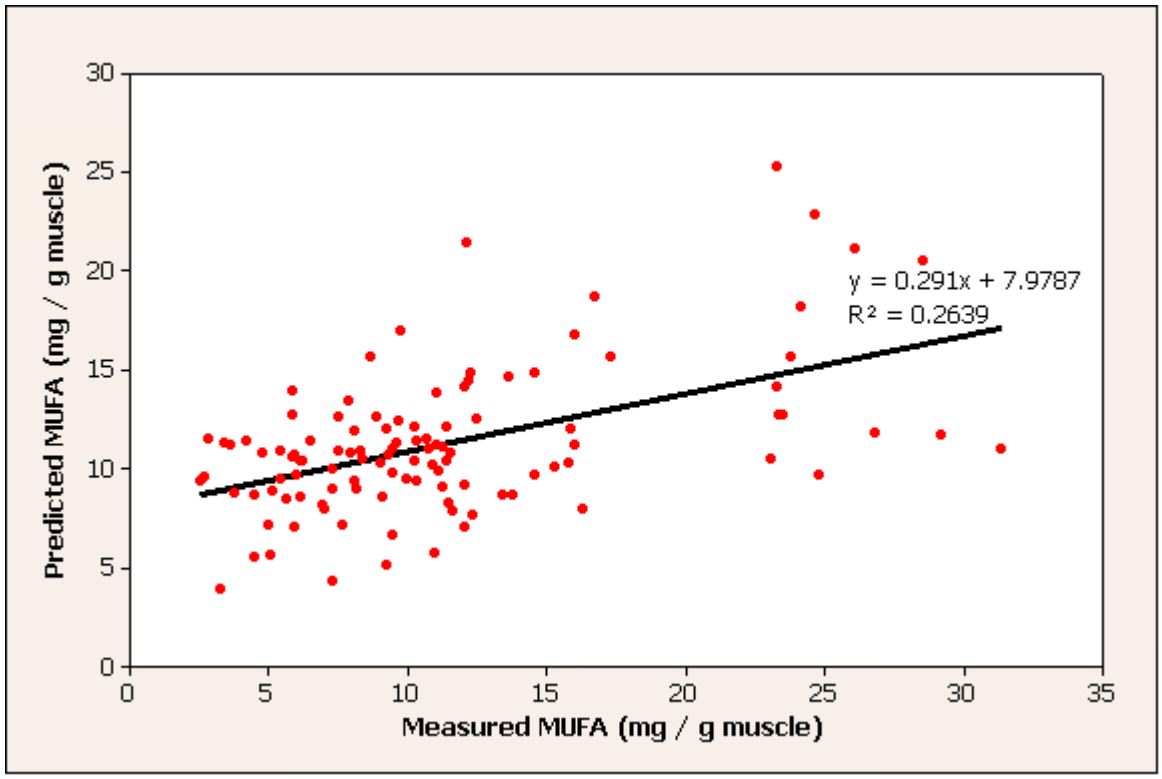

Figure 30 – Relationship between measured SFA and SFA predicted by Raman Spectroscopy

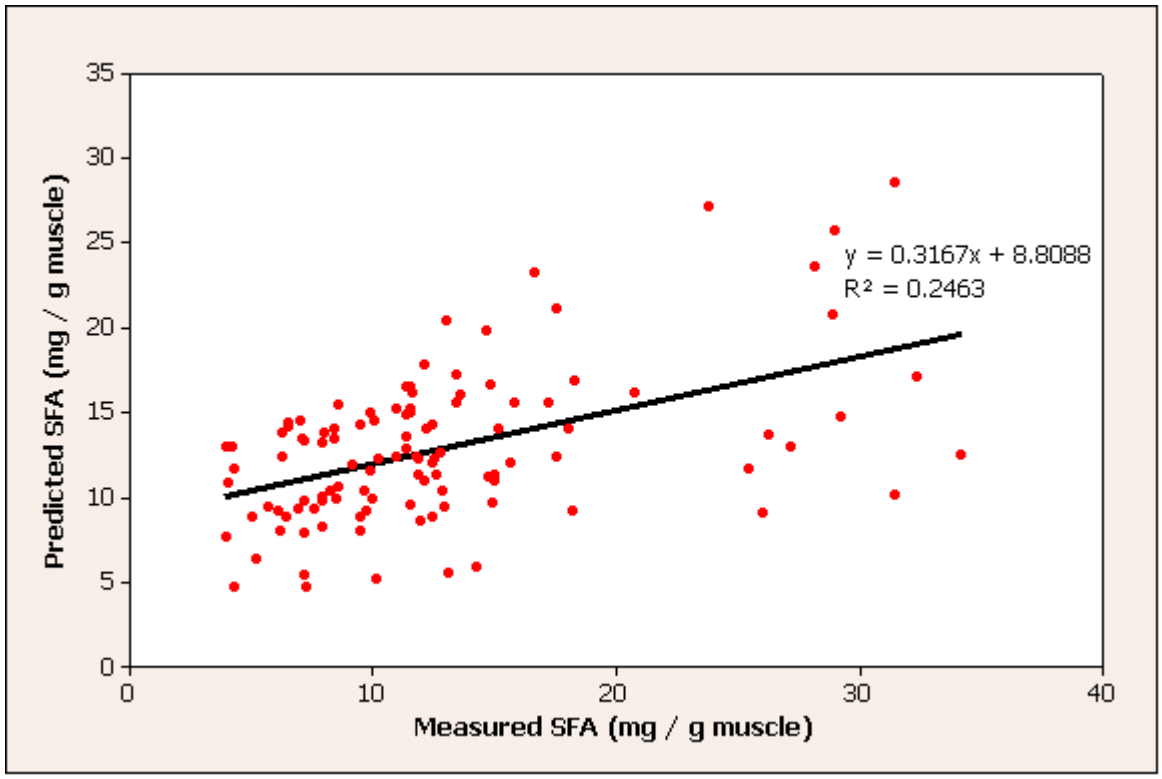

Figure 31 – Relationship between measured CLA and CLA predicted by Raman Spectroscopy

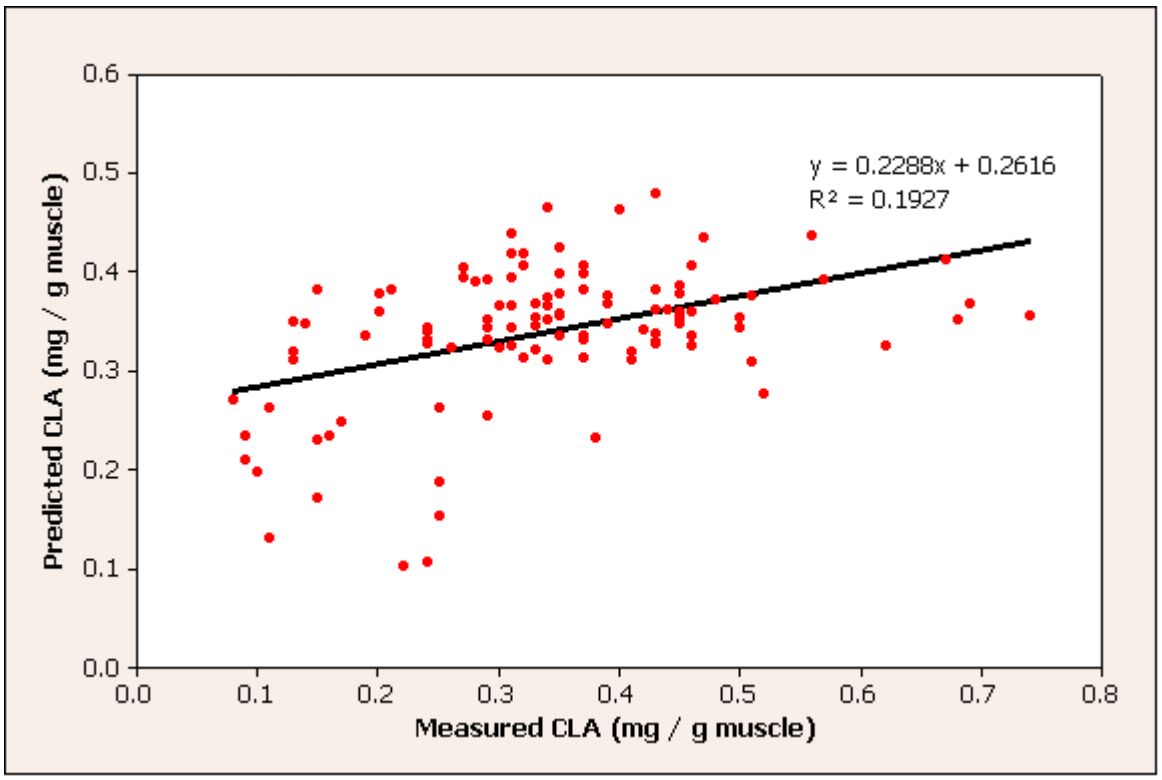

11 Appendix 4 Fatty acid groups definition

Table 13 – Fatty acids used in calculation of fatty acid
(a √ indicates fatty acids used in calculation of fatty acid groups)

	Fatty Acid Groups				
	SFA	MUFA	PUFA	CLA	*Trans*‡
C12:0	√				
C13:0	√				
C14:0	√				
C14:1*c*9		√			
C15:0	√				
C15:1*c*		√			
C16:0	√				
C16:1*t*9					√
C16:1*c*9		√			
C17:0	√				
C17:1*c*		√			
C18:0	√				
C18:1*t*9					√
C18:1*t*11					√
C18:1*c*9		√			
C18:1*c*11		√			
C18:2*t*9,*t*12					√
C18:2*c*9,*c*12 (*n*6)			√		
C18:3 *c*9,*c*12,*c*15 (*n*3)			√		
CLA*c*9,*t*11				√	
CLA*t*10,*c*12				√	√
C20:4*n*6			√		
C20:5*n*3			√		
C22:5*n*3			√		
C22:6*n*3			√		

All MUFA and PUFA included in predictions were cis fatty acids
‡ CLA c9, t12 may also be included here